

Quantized fixed-time fault-tolerant attitude control for hypersonic reentry vehicles



Tiancai Wu^{a,b,c}, Honglun Wang^{a,b,*}, Yue Yu^d, Yiheng Liu^{a,b,c}, Jianfa Wu^{a,b,c}

^a School of Automation Science and Electrical Engineering, Beihang University, Beijing 100191, China

^b Science and Technology on Aircraft Control Laboratory, Beihang University, Beijing 100191, China

^c Shenyuan Honors College, Beihang University, Beijing 100191, China

^d Beijing Aerospace Automatic Control Institute, Beijing 100191, China

ARTICLE INFO

Article history:

Received 20 December 2020

Revised 23 April 2021

Accepted 29 April 2021

Available online 19 May 2021

Keywords:

Hypersonic reentry vehicle

Fault-tolerant control

Fixed-time convergence

Signal quantization

ABSTRACT

A quantized fixed-time fault-tolerant attitude control problem for hypersonic reentry vehicles is considered from the perspective of practical engineering. Taking into account the limited time available for recovery from a fault scenario, fixed-time extended state observers are used to simultaneously compensate for the negative effect of unknown time-varying actuator faults, uncertainties, and external disturbances. In contrast to the existing control schemes, which neglect the signal quantization transmission process and limited communication capacity, the hysteresis quantization mechanism is considered. Based on this, a fixed-time fault-tolerant control scheme is developed to ensure the fixed time convergence of all the tracking errors even in cases involving actuator faults. The stability and convergence are proven by performing a theoretical analysis. The simulation results validate the superiority and robustness of the proposed control scheme.

© 2021 Elsevier Inc. All rights reserved.

1. Introduction

In recent years, hypersonic reentry vehicles (HRVs), which exhibit unique advantages of fast flight capability and strong maneuverability, have attracted considerable attention in both civil and military fields [1]. However, to compensate for certain inherent limitations, i.e., substantial uncertainties, tight coupling, and unknown external disturbances, the control system for HRVs must exhibit a fast response and anti-disturbance capability [2]. Hence, the design of the attitude controller for HRVs is a key yet challenging issue. In this regard, active disturbance rejection control [3], back-stepping control [4], and sliding mode control [5,6] have been employed to ensure the attitude control performance of HRVs. Moreover, with the development of intelligent technologies, intelligence-based control methods, such as adaptive-based control [7], fuzzy-based control [8,9], neural network-based control [10], and deep neural network-based control [11–13], have attracted significant attention and been widely used to enhance the control performance.

Moreover, in the practical flight process of HRVs, actuator faults may be encountered due to the severe environment, which may lead to unpredictable accidents [14,15]. Consequently, the research on the fault-tolerant control (FTC) for HRVs has been prioritized to satisfy the increasingly stringent requirements regarding the safety and reliability of such safety-critical systems [16].

* Corresponding author: School of Automation Science and Electrical Engineering, Beihang University, Beijing 100191, China.
E-mail addresses: wutic@buaa.edu.cn (T. Wu), wang_hl_12@126.com (H. Wang), yuyuehkp@sina.com (Y. Yu).

In recent decades, many advanced FTC strategies with different features have been employed to address the abovementioned control issue. An et al. [16] proposed an FTC scheme for hypersonic vehicles, in which a disturbance observer was used to compensate for the effect of actuator faults. Hu et al. [17] combined the classic dynamic surface control with an adaptive method and a bound estimation approach to ensure the control performance under time-varying actuator faults. Furthermore, the fuzzy logic system and neural network were adopted as intelligent approaches to address the FTC problem [18,19]. Nevertheless, although these approaches could exhibit an excellent control performance under actuator faults, only the asymptotic stability of the closed-loop system could be ensured. In other words, all the error variables converged within an infinite time. Notably, for a safety-critical and fast time-varying system as the control system of the HRV, if the compensation for the negative effect of the actuator faults exceeds the allowable time, the system is likely to collapse [20]. To enhance the fast convergence of control systems, a fixed-time observer-based finite-time FTC was established for hypersonic gliding vehicles (HGVs) [21], and an integral terminal sliding-mode control integrated with adaptive techniques was developed for the HGV, which could drive the convergence of all the error variables within a finite-time [22].

Furthermore, in the existing methods, the convergence time depended strictly on the values of the initial conditions. In such a scenario, if the initial state is far from the origin, the convergence time likely tends to infinity. This defect severely hinders the practical application of the finite-time method. Consequently, a fixed-time control method was proposed for quadrotors, based on the fixed-time theory and bi-limit homogeneity property, and all the error variables were demonstrated to be fixed-time convergent [23]. Moreover, a fixed-time accommodation strategy for actuator faults was presented for HGVs, although the convergence time of the sliding phase could not be obtained directly [20]. Overall, designing a fixed-time FTC scheme with a predefined bounded convergence time for HRVs is significant yet challenging.

Additionally, most of the existing control schemes assumed that the control signals could be transmitted to the actuator modules in real time without deviations, and the communication capability was sufficient. However, in the existing digital control systems, the practical signal quantization transmission process and limited communication capacity cannot be ignored, especially in the case of resource constrained systems. Wang et al. [15] proposed an event-triggered attitude control scheme for fractionated spacecraft with wireless communication to reduce the communication burden. A hysteresis quantizer (HQ) was synthesized into the controller design to reduce the actuator bandwidth for the micro-electro-mechanical system (MEMS) gyroscope [24]. Based on the event-triggered mechanism, intermittent-measurement-involved extended state observers and controllers were developed for flexible HFVs involving limited resources [25]. Furthermore, an adaptive control with a logarithmic quantization mechanism was implemented to realize the tracking control of HFVs [26]; however, the logarithmic quantizer could lead to chattering, which may deteriorate the control performance and system stability.

Furthermore, during HRV missions, which are characteristically long distance and long endurance, the energy of the HRVs cannot be replenished. For such systems with limited resources, the problem of signal quantization transmission and limited communication capacity must be considered when designing the controller, and this aspect requires additional research.

Considering these aspects, this paper proposes a fixed-time fault-tolerant attitude control strategy for HRVs, which takes into account the quantization mechanism. The main contributions of this paper can be summarized as follows:

- (1) Different from the existing asymptotic convergence and finite-time convergence fault compensation techniques [16,19], fixed-time extended state observers (FESOs) are employed to simultaneously estimate the lumped disturbances including unknown time-varying actuator faults, uncertainties, and external disturbances. Particularly, the adopted FESOs can not only estimate the negative effect of the lumped disturbances within a predefined time but also enhance the robustness of the closed-loop control system in fault scenarios.
- (2) In contrast to the previous studies [21,16–20,22], the signal quantization transmission process and limited communication capacity are considered. A hysteresis quantization mechanism is implemented in the proposed control scheme to effectively reduce the communication load and save communication resources in the controller-to-actuator channel for limited resource systems.
- (3) A non-singular terminal sliding mode surface-based fixed-time control strategy is proposed to ensure that all the error variables can converge within a predetermined time. In contrast to the previous fixed-time control protocols [23,27], in which the convergence time could not be obtained directly, the convergence time in the proposed control strategy can be directly estimated by considering the controller parameters, independent of the different initial states.

The remainder of this paper is organized as follows. The modeling of the HRV and actuator and problem formulation are described in Section 2. The design of the quantized fixed-time fault-tolerant scheme and stability analysis are presented in Section 3. The simulation results and corresponding discussion are described in Section 4, and the concluding remarks are presented in Section 5.

2. Problem formulation

2.1. Mathematical model of the hrv

The HRV model used in this paper is with reference to that reported in [28,29]. The HRV model adopts the winged-cone geometry, and its configuration and structural parameters are shown in Fig. 1 and Table 1, respectively.

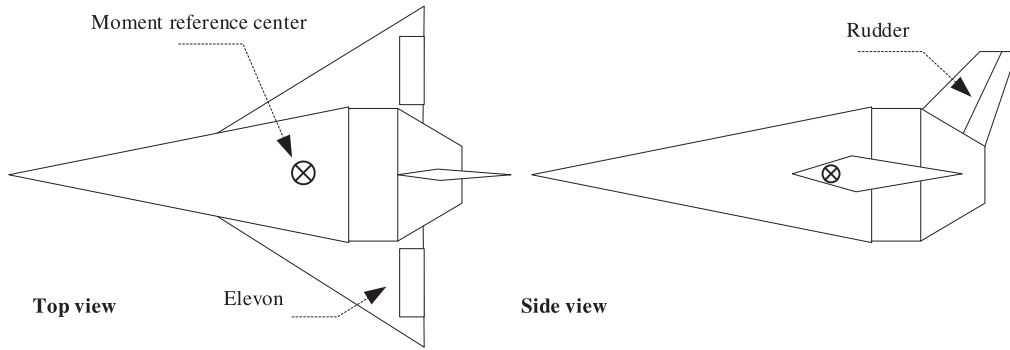


Fig. 1. Three views of the HRV model.

Table 1
Geometric characteristics of the HRV model.

	Notation	Unit	Parameters
Mass	m	kg	63,500
Reference area	S	m ²	334.73
Span	b	m	18.29
Mean aerodynamic chord	c	m	24.38
Roll moment of inertia	I_x	kg · m ²	915,300
Pitch moment of inertia	I_z	kg · m ²	903,600
Yaw moment of inertia	I_y	kg · m ²	903,600

Due to the limitation of the length of the paper, only the parameters that are used in the design of the control system are listed in Table 1. The remaining structural parameters and fitting polynomials of the aerodynamic coefficients, which are not listed herein, can be found in [28,29].

Based on the assumption of a uniform gravitational field and a rigid vehicle structure, the nonlinear motion equations of the HRV can be described as

$$\begin{cases} \dot{r}_e = V \sin \theta \\ \dot{\phi} = \frac{V \cos \theta \sin \psi_s}{r_e \cos \varphi} \\ \dot{\varphi} = \frac{V \cos \theta \cos \psi_s}{r_e} \end{cases} \quad (1)$$

$$\begin{cases} \dot{V} = \frac{-D - mg \sin \theta}{m} + \omega_e^2 r_e \cos \varphi (\sin \theta \cos \varphi - \cos \theta \sin \varphi \cos \psi_s) \\ \dot{\psi}_s = -\frac{L \sin \gamma_s + Z \cos \gamma_s}{mV \cos \theta} + \frac{V}{r_e} \cos \theta \sin \psi_s \tan \varphi - 2\omega_e (\tan \theta \cos \varphi \cos \psi_s - \sin \varphi) \\ \quad + \frac{\omega_e^2 r_e}{V \cos \theta} \sin \varphi \cos \varphi \sin \psi_s \\ \dot{\theta} = \frac{L \cos \gamma_s - mg \cos \theta}{mV} + \frac{V}{r_e} \cos \theta + 2\omega_e \cos \varphi \sin \psi_s \\ \quad + \frac{\omega_e^2 r_e \cos \varphi}{V} (\cos \theta \cos \varphi + \sin \theta \sin \varphi \cos \psi_s) \end{cases} \quad (2)$$

$$\begin{cases} \dot{\alpha} = -w_x \cos \alpha \tan \beta + w_y \sin \alpha \tan \beta + w_z + \frac{mg \cos \theta \cos \gamma_s - L}{mV \cos \beta} \\ \dot{\beta} = w_x \sin \alpha + w_y \cos \alpha + \frac{mg \cos \theta \sin \gamma_s - Z \cos \beta}{mV} \\ \dot{\gamma}_s = w_x \cos \alpha \sec \beta - w_y \sin \alpha \sec \beta - \frac{g \cos \theta \cos \gamma_s \tan \beta}{V} \\ \quad + \frac{L(\tan \theta \sin \gamma_s + \tan \beta) + Z \tan \theta \cos \gamma_s}{mV} \end{cases} \quad (3)$$

$$\begin{cases} \dot{w}_x = \frac{I_y - I_z}{I_x} w_y w_z + \frac{M_x}{I_x} \\ \dot{w}_y = \frac{I_z - I_x}{I_y} w_z w_x + \frac{M_y}{I_y} \\ \dot{w}_z = \frac{I_x - I_y}{I_z} w_x w_y + \frac{M_z}{I_z} \end{cases} \quad (4)$$

where r_e is the radial distance from the Earth center to the vehicle, φ, ϕ are the longitude and latitude, respectively, ω_e denote the Earth rotating rate, V, ψ_s, θ denote the velocity, heading angle, and flight path angle, respectively, α, β, γ_s denote the angles of attack, sideslip, and bank, respectively, w_x, w_y, w_z denote the roll angular rate, yaw angular rate, and pitch angular rate, respectively, and g is the gravitational acceleration.

The aerodynamic forces L, D and Z can be defined as

$$\begin{cases} L = QSC_L \\ D = QSC_D \\ Z = QSC_Z \end{cases} \quad (5)$$

where $C_L=C_{L,\alpha} + C_{L,\delta_e} + C_{L,\delta_a}$, $C_D=C_{D,\alpha} + C_{L,\delta_e} + C_{L,\delta_a} + C_{L,\delta_r}$, and $C_Z=C_{Z,\beta} + C_{Z,\delta_e} + C_{Z,\delta_a} + C_{Z,\delta_r}$ are the lift, drag, and side force coefficients, respectively, and $\delta_e, \delta_a, \delta_r$ denote the left elevon, right elevon, and rudder, respectively.

The aerodynamic moments M_x, M_y and M_z can be defined as

$$\begin{cases} M_x=Q S b m_x \\ M_y=Q S b m_y \\ M_z=Q S c m_z - x_{cg}(-D \sin \alpha - L \cos \alpha) \end{cases} \quad (6)$$

where $m_x=m_x^\beta \beta + m_x^{\delta_e} \delta_e + m_x^{\delta_a} \delta_a + m_x^{\delta_r} \delta_r + m_x^{w_x} \frac{w_x b}{2V} + m_x^{w_y} \frac{w_y b}{2V}$, $m_y=m_y^\beta \beta + m_y^{\delta_e} \delta_e + m_y^{\delta_a} \delta_a + m_y^{\delta_r} \delta_r + m_y^{w_x} \frac{w_x b}{2V} + m_y^{w_y} \frac{w_y b}{2V}$, and $m_z=m_{z,\alpha} + m_z^{\delta_e} \delta_e + m_z^{\delta_a} \delta_a + m_z^{\delta_r} \delta_r + m_z^{w_z} \frac{w_z c}{2V}$ are the roll, yaw, and pitch moment coefficients, respectively.

Furthermore, in ground wind tunnel experiments, it is difficult to simulate a high Mach flight environment, which may result in uncertainties in the aerodynamics parameters. Considering the uncertainties, the aerodynamic force and moment coefficients can be represented as:

$$\begin{cases} C_i=\bar{C}_i(1+\Delta_F) \\ m_j=\bar{m}_j(1+\Delta_M) \end{cases} \quad (7)$$

where $i=L, D, Z, j=x, y, z$, \bar{C}_i and \bar{m}_j denote the nominal values of the aerodynamic force and moment coefficients, respectively. The fitting polynomial expressions of the aerodynamic force and moment coefficients can be found in [28,29]. Δ_F and Δ_M represent the perturbation ranges of the aerodynamic force and moment coefficients, respectively.

To facilitate the design of the attitude control system, the attitude angle state, angular rate state, and control input are defined as $\Omega=[\alpha, \beta, \gamma_s]^T$, $\omega=[w_x, w_y, w_z]^T$ and $\mathbf{u}=[\delta_e, \delta_a, \delta_r]^T$, respectively. And the aerodynamic force generated by the deflection angles is negligible. The equations for the attitude kinematics and dynamics (3)-(4) can be rewritten in the following affine nonlinear matrix form:

$$\begin{cases} \dot{\Omega}=\mathbf{f}_\Omega+\mathbf{g}_\Omega \omega+\Delta_\Omega \\ \dot{\omega}=\mathbf{f}_\omega+\mathbf{g}_\omega \mathbf{u}+\Delta_\omega \end{cases} \quad (8)$$

where Δ_Ω and Δ_ω represent the lumped disturbances in the attitude angle loop and angular rate loop, respectively, \mathbf{g}_Ω and \mathbf{g}_ω can be described as

$$\mathbf{g}_\Omega=\begin{bmatrix} -\cos \alpha \tan \beta & \sin \alpha \tan \beta & 1 \\ \sin \alpha & \cos \alpha & 0 \\ \cos \alpha \sec \beta & -\sin \alpha \sec \beta & 0 \end{bmatrix}, \mathbf{g}_\omega=\begin{bmatrix} Q S b m_x^{\delta_e} / I_x & Q S b m_x^{\delta_a} / I_x & Q S b m_x^{\delta_r} / I_z \\ Q S b m_y^{\delta_e} / I_y & Q S b m_y^{\delta_a} / I_y & Q S b m_y^{\delta_r} / I_y \\ Q S c m_z^{\delta_e} / I_z & Q S c m_z^{\delta_a} / I_z & Q S c m_z^{\delta_r} / I_z \end{bmatrix} \quad (9)$$

$\mathbf{f}_\Omega=[f_\alpha, f_\beta, f_{\gamma_s}]^T$ and $\mathbf{f}_\omega=[f_{w_x}, f_{w_y}, f_{w_z}]^T$ can be described as

$$\begin{cases} f_\alpha=g \cos \theta \cos \gamma_s / (V \cos \beta) - Q S \bar{C}_{L,\alpha} / (m V \cos \beta) \\ f_\beta=g \cos \theta \sin \gamma_s / V - Q S \bar{C}_Z^\beta \beta \cos \beta / (m V) \\ f_{\gamma_s}=-g \cos \theta \cos \gamma_s \tan \beta / V + \left(Q S \bar{C}_Z^\beta \beta \tan \theta \cos \gamma_s + Q S \bar{C}_{L,\alpha} (\tan \theta \sin \gamma_s + \tan \beta) \right) / (m V) \\ f_{w_x}=(I_y-I_z) w_y w_z / I_x + Q S b \left(m_x^\beta \beta + \left(m_x^{w_x} w_x b + m_x^{w_y} w_y b \right) / (2 V) \right) / I_x \\ f_{w_y}=(I_z-I_x) w_z w_x / I_y + Q S b \left(m_y^\beta \beta + \left(m_y^{w_x} w_x b + m_y^{w_y} w_y b \right) / (2 V) \right) / I_y \\ f_{w_z}=(I_x-I_y) w_y w_z / I_z + Q S c \left(m_{z,\alpha} + m_z^{w_z} w_z c / (2 V) \right) / I_z \end{cases} \quad (10)$$

$\Delta_\Omega=[\Delta_\alpha, \Delta_\beta, \Delta_{\gamma_s}]^T$ and $\Delta_\omega=[\Delta_{w_x}, \Delta_{w_y}, \Delta_{w_z}]^T$ can be described as

$$\begin{cases} \Delta_\alpha=-Q S \Delta_F \bar{C}_L / (m V \cos \beta) + d_\alpha \\ \Delta_\beta=-Q S \Delta_F \bar{C}_Z \cos \beta / (m V) + d_\beta \\ \Delta_{\gamma_s}=\left(Q S \Delta_F \bar{C}_Z \tan \theta \cos \gamma_s + Q S \Delta_F \bar{C}_L (\tan \theta \sin \gamma_s + \tan \beta) \right) / (m V) + d_{\gamma_s} \\ \Delta_{w_x}=Q S b \Delta_M \bar{m}_x / I_x + d_{w_x} \\ \Delta_{w_y}=Q S b \Delta_M \bar{m}_y / I_y + d_{w_y} \\ \Delta_{w_z}=Q S c \Delta_M \bar{m}_z / I_z - x_{cg}(-Q S \Delta_F \bar{C}_D \sin \alpha - Q S \Delta_F \bar{C}_L \cos \alpha) + d_{w_z} \end{cases} \quad (11)$$

where $d_\alpha, d_\beta, d_{\gamma_s}, d_{w_x}, d_{w_y}$, and d_{w_z} denote the external disturbances.

2.2. Mathematical model of the actuator

This subsection describes the establishment of the mathematical model of the actuator faults and HQ.

The effectiveness loss fault and bias fault commonly occur in the HRV, and thus, the general actuator fault model of the HRV can be expressed as [20]

$$\mathbf{u}=\lambda \mathbf{u}_c+\boldsymbol{\varsigma} \quad (12)$$

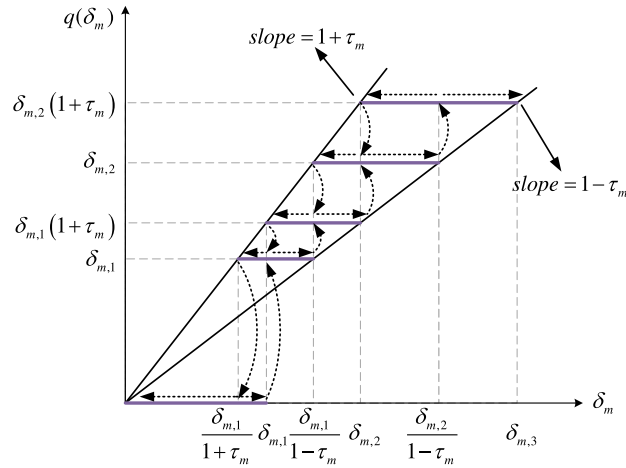


Fig. 2. Mapping between $q(\delta_m)$ and δ_m when $\delta_m > 0$.

where $\mathbf{u} = [\delta_e, \delta_a, \delta_r]^T$ is the actual actuator deflection, $\mathbf{u}_c = [\delta_{ec}, \delta_{ac}, \delta_{rc}]^T$ represents the desired control signal, $\boldsymbol{\lambda} = \text{diag}\{\lambda_e, \lambda_a, \lambda_r\}$, ($0 < \lambda_i \leq 1, i = e, a, r$) denotes the effectiveness loss faults, and $\boldsymbol{\zeta} = \text{diag}\{\zeta_e, \zeta_a, \zeta_r\}$ denotes the bias faults. In this work, λ_i and ζ_i are represented by time-varying functions, which have a wider applicability.

The HQ in the controller-to-actuator channel is defined as follows [30]:

$$q(\delta_m) = \begin{cases} \delta_{m,i} \text{sgn}(\delta_m), \frac{\delta_{m,i}}{1+\tau_m} < |\delta_m| \leq \delta_{m,i}, \dot{\delta}_m < 0, \text{ or} \\ \delta_{m,i} < |\delta_m| \leq \frac{\delta_{m,i}}{1-\tau_m}, \dot{\delta}_m > 0 \\ \delta_{m,i}(1+\tau_m) \text{sgn}(\delta_m), \delta_{mi} < |\delta_m| \leq \frac{\delta_{m,i}}{1-\tau_m}, \dot{\delta}_m < 0, \text{ or} \\ \frac{\delta_{m,i}}{1-\tau_m} < |\delta_m| \leq \frac{\delta_{m,i}(1+\tau_m)}{1-\tau_m}, \dot{\delta}_m > 0 \\ 0, 0 \leq |\delta_m| < \frac{\delta_{m,\min}}{1+\tau_m}, \dot{\delta}_m < 0, \text{ or} \\ \frac{\delta_{m,\min}}{1+\tau_m} \leq |\delta_m| \leq \delta_{m,\min}, \dot{\delta}_m > 0 \\ q(\delta_m(t^-)), \dot{\delta}_m = 0 \end{cases} \quad (13)$$

where $\delta_{m,i} = \rho_m^{1-i} \delta_{m,\min}$ with integer $i = 1, 2, \dots, m = e, a, r$ denotes the left elevon, right elevon, and rudder, respectively, $\delta_{m,\min} > 0$ denotes the size of the dead zone of $q(\delta_m)$, $0 < \rho_m < 1$ is a measure of the quantization density and used to define $\tau_m = (1 - \rho_m)/(1 + \rho_m)$, $\delta_m(t^-)$ denotes the actuator deflection at the last moment, and $q(\delta_m)$ lies in the set $\{0, \pm \delta_{m,i}, \pm \delta_{m,i}(1 + \tau_m)\}$. Fig. 2 shows the mapping relationship between $q(\delta_m)$ and δ_m when $\delta_m > 0$.

Based on the quantization decomposition technique reported in [31], the output $q(\delta_m)$ of the HQ can be decomposed into the following form:

$$q(\delta_m) = H(\delta_m)\delta_m + L(\delta_m) \quad (14)$$

where

$$H(\delta_m) = \begin{cases} q(\delta_m)/\delta_m, q(\delta_m) \neq 0 \\ 1, q(\delta_m) = 0 \end{cases}, L(\delta_m) = \begin{cases} 0, q(\delta_m) \neq 0 \\ -\delta_m, q(\delta_m) = 0 \end{cases}$$

Lemma 1 [31]. In the decomposition specified in (14), the control coefficient $H(\delta_m)$ and disturbance-like term $L(\delta_m)$ satisfy the following inequality:

$$1 - \tau_m \leq H(\delta_m) \leq 1 + \tau_m, |L(\delta_m)| \leq \delta_{m,\min} \quad (15)$$

Considering the actuator faults and HQ and substituting (12) and (13) into (8) yields

$$\begin{aligned} \dot{\boldsymbol{\omega}} &= \mathbf{f}_\omega + \mathbf{g}_\omega(\boldsymbol{\lambda}\mathbf{Q}(\mathbf{u}) + \boldsymbol{\zeta}) + \Delta_\omega \\ &= \mathbf{f}_\omega + \mathbf{g}_\omega\mathbf{Q}(\mathbf{u}) + \mathbf{g}_\omega((\boldsymbol{\lambda} - \mathbf{E})\mathbf{Q}(\mathbf{u}) + \boldsymbol{\zeta}) + \Delta_\omega \end{aligned} \quad (16)$$

where $\mathbf{Q}(\mathbf{u}) = [q(\delta_e), q(\delta_a), q(\delta_r)]^T$ denotes the quantized input and \mathbf{E} represents the identity matrix.

Consequently, the control-oriented model can be represented as:

$$\begin{cases} \dot{\boldsymbol{\Omega}} = \mathbf{f}_\Omega + \mathbf{g}_\Omega\boldsymbol{\omega} + \Delta_\Omega \\ \dot{\boldsymbol{\omega}} = \mathbf{f}_\omega + \mathbf{g}_\omega\mathbf{Q}(\mathbf{u}) + \Delta_{\omega f} \end{cases} \quad (17)$$

where $\Delta_{\omega f} = \mathbf{g}_\omega((\boldsymbol{\lambda} - \mathbf{E})\mathbf{Q}(\mathbf{u}) + \boldsymbol{\zeta}) + \Delta_\omega = [\Delta_{w_x f}, \Delta_{w_y f}, \Delta_{w_z f}]^T$ denotes the lumped disturbances in the angular rate loop.

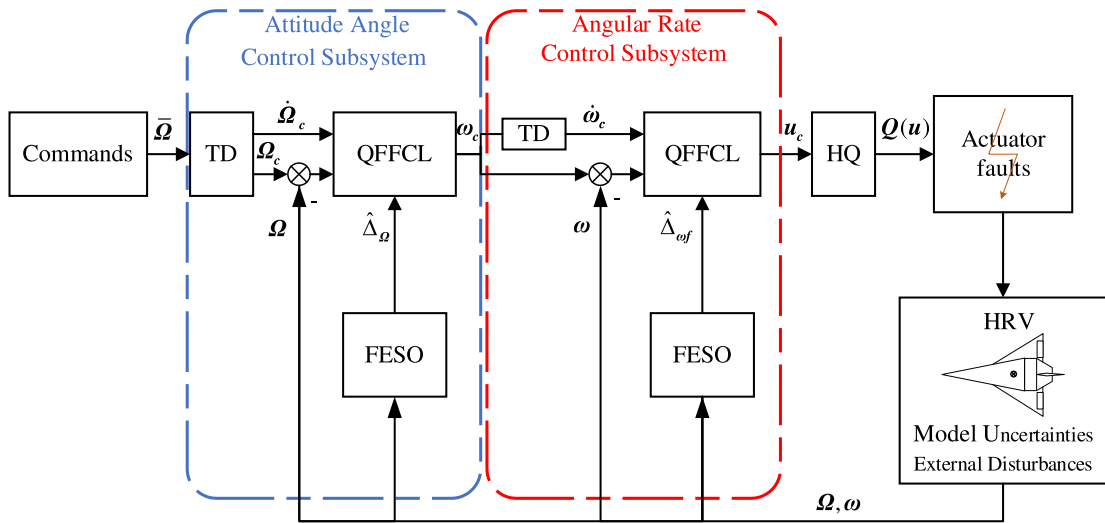


Fig. 3. Structure of the proposed controller.

Assumption 1. [32]: The lumped disturbances $\Delta_i(i = \Omega, \omega f)$ and their first-order derivatives are bounded, such that $\|\Delta_i\| \leq M_i, \|\dot{\Delta}_i\| \leq L_i$.

Control Objective: The control objective of this paper is to design a quantized fixed-time fault-tolerant scheme such that the system states can track the desired instructions Ω_c and ω_c within a fixed time in the presence of actuator faults, uncertainties, and external disturbances and effectively reduce the communication load.

3. Design of the quantized fixed-time FTC scheme

This section describes the controller design process. The structure of the proposed controller is shown in Fig. 3. According to the time-scale separation and singular perturbation theory, the attitude system of an HRV can be divided into an attitude angle control subsystem and angular rate control subsystem [32]. The attitude angle control subsystem tracks the attitude angle command and generates the virtual reference command for the angular rate control subsystem. The angular rate control subsystem tracks the virtual angular rate command generated by the former subsystem and generates the actuators' deflection signal. Note that the actuator input signal is quantized by the HQ, and the actuator faults are considered in this paper. Fig. 3 shows that the two control subsystems have similar control structures. Nonlinear first-order filters (NFFs) are employed to generate more realizable command signals and corresponding differential signals. Moreover, the "differential explosion" problem can be avoided in this manner. FESOs are introduced to estimate the lumped disturbances within a fixed time. Quantized fixed-time FTC laws (QFFCLs) are designed to ensure the closed-loop control performance.

Notation 1. In this paper, for all $\mathbf{x} = [x_1, x_2, \dots, x_n]^T \in \mathbb{R}^n \times 1$, the symbol $\text{sig}^q(\mathbf{x})$ denotes $[|x_1|^q \cdot \text{sgn}(x_1), \dots, |x_n|^q \cdot \text{sgn}(x_n)]^T$, where $\text{sgn}(\cdot)$ represents the sign function.

3.1. Controller design for the attitude angle subsystem

3.1.1. Design of the NFF

Lemma 2 [33]. Consider the following nonlinear system:

$$\dot{\sigma} = -k_1 \text{sig}^{q_1}(\sigma) - k_2 \text{sig}^{q_2}(\sigma), \sigma(0) = \sigma_0 \tag{18}$$

where $q_1 > 1, 0 < q_2 < 1, k_1, k_2 > 0$. In this case, system (18) is fixed-time stable, and the settling time $T(\sigma_0)$ can be bounded as follows:

$$T(\sigma_0) \leq T_{\max} = \frac{1}{k_1(1 - q_1)} + \frac{1}{k_2(q_2 - 1)} \tag{19}$$

To avoid the actuator saturation caused by drastic changes in the reference command $\bar{\omega} = [\bar{\alpha}, \bar{\beta}, \bar{\gamma}_s]^T$, the NFF is employed to generate a more realizable command signal $\Omega_c = [\alpha_c, \beta_c, \gamma_{sc}]^T$ and corresponding differential signal $\dot{\Omega}_c$, which are used in the design of the QFFCL.

$$\tau_{\Omega F} \dot{\Omega}_c = -\text{sig}^{\alpha_{\Omega F}}(\Omega_c - \bar{\omega}) - \text{sig}^{\beta_{\Omega F}}(\Omega_c - \bar{\omega}) \tag{20}$$

where $\tau_{\Omega F}$ is a small positive constant; $\alpha_{\Omega F} \in (0, 1)$, and $\beta_{\Omega F} > 1$. According to Lemma 2, the NFF can ensure overall fixed-time convergence [33]. The error of the NFF in the attitude angle subsystem can be defined as $\varepsilon_{\Omega} = \Omega_c - \bar{\omega}$.

3.1.2. Design of the FESO

This subsection describes the design of the FESO used to estimate the lumped disturbances in the attitude angle subsystem within a fixed time. The FESO is formulated as follows [34]:

$$\begin{cases} \dot{\tilde{\mathbf{e}}}_\Omega = \hat{\mathbf{\Omega}} - \mathbf{\Omega} \\ \dot{\hat{\mathbf{\Omega}}} = \mathbf{f}_\Omega + \mathbf{g}_\Omega \boldsymbol{\omega} - \mu_{\Omega 01} \text{sig}^{\alpha_{\Omega 01}}(\tilde{\mathbf{e}}_\Omega) - \mu_{\Omega 02} \text{sig}^{\beta_{\Omega 01}}(\tilde{\mathbf{e}}_\Omega) + \hat{\Delta}_\Omega \\ \dot{\hat{\Delta}}_\Omega = -\mu_{\Omega 03} \text{sig}^{\alpha_{\Omega 02}}(\tilde{\mathbf{e}}_\Omega) - \mu_{\Omega 04} \text{sig}^{\beta_{\Omega 02}}(\tilde{\mathbf{e}}_\Omega) - \chi_{\Omega 0} \text{sign}(\tilde{\mathbf{e}}_\Omega) \end{cases} \quad (21)$$

where $\hat{\mathbf{\Omega}}$ and $\hat{\Delta}_\Omega$ represent the estimates of the attitude angle $\mathbf{\Omega}$ and lumped disturbances Δ_Ω , respectively, $\tilde{\mathbf{e}}_\Omega$ denotes the estimation error, and $\alpha_{\Omega 01} \in (0, 1)$, $\beta_{\Omega 01} > 1$, $\alpha_{\Omega 02} = 2\alpha_{\Omega 01} - 1$, $\beta_{\Omega 02} = 2\beta_{\Omega 01} - 1$, $\chi_{\Omega 0} > L_\Omega$, and $\mu_{\Omega 0i} > 0 (i = 1, 2, 3, 4)$ are the observer parameters to be designed.

Theorem 1. Suppose that the lumped disturbances Δ_Ω satisfy Assumption 1, and the FESO is designed as indicated in (21). The lumped disturbances Δ_Ω can be estimated within a fixed time by the FESO, and the upper bound on the convergence time $T_{\Omega 0}$ can be estimated as follows:

$$T_{\Omega 0} \leq \frac{\lambda_{\max}(\Sigma_{\Omega 1})^{(1-\alpha_{\Omega 01})}}{\lambda_{\Omega 1}(1-\alpha_{\Omega 01})} + \frac{1}{\lambda_{\Omega 2}(\beta_{\Omega 01}-1)\varpi_\Omega^{(\beta_{\Omega 01}-1)}} \quad (22)$$

where $\lambda_1 = \lambda_{\min}(Q_{\Omega 1})/\lambda_{\max}(\Sigma_{\Omega 1})$, $\lambda_2 = \lambda_{\min}(Q_{\Omega 2})/\lambda_{\max}(\Sigma_{\Omega 2})$, $\lambda_{\min}(\Sigma_{\Omega 2}) \geq \varpi_\Omega > 0$, and $Q_{\Omega 1}, \Sigma_{\Omega 1}, Q_{\Omega 2}, \Sigma_{\Omega 2}$ are positive definite matrices that satisfy

$$\begin{aligned} \Sigma_{\Omega 1} P_{\Omega 1} + P_{\Omega 1}^T \Sigma_{\Omega 1} &= -Q_{\Omega 1}, \Sigma_{\Omega 2} P_{\Omega 2} + P_{\Omega 2}^T \Sigma_{\Omega 2} = -Q_{\Omega 2} \\ P_{\Omega 1} &= \begin{bmatrix} -\mu_{\Omega 01} & 1 \\ -\mu_{\Omega 03} & 0 \end{bmatrix}, P_{\Omega 2} = \begin{bmatrix} -\mu_{\Omega 02} & 1 \\ -\mu_{\Omega 04} & 0 \end{bmatrix} \end{aligned} \quad (23)$$

Proof. First, we define the following error variables:

$$\begin{cases} \tilde{\mathbf{e}}_\Omega = \hat{\mathbf{\Omega}} - \mathbf{\Omega} \\ \tilde{\Delta}_\Omega = \hat{\Delta}_\Omega - \Delta_\Omega \end{cases} \quad (24)$$

By obtaining the derivative of (21), the error dynamic system can be defined as follows:

$$\begin{cases} \dot{\tilde{\mathbf{e}}}_\Omega = \tilde{\Delta}_\Omega - \mu_{\Omega 01} \text{sig}^{\alpha_{\Omega 01}}(\tilde{\mathbf{e}}_\Omega) - \mu_{\Omega 02} \text{sig}^{\beta_{\Omega 01}}(\tilde{\mathbf{e}}_\Omega) \\ \dot{\tilde{\Delta}}_\Omega = -\mu_{\Omega 03} \text{sig}^{\alpha_{\Omega 02}}(\tilde{\mathbf{e}}_\Omega) - \mu_{\Omega 04} \text{sig}^{\beta_{\Omega 02}}(\tilde{\mathbf{e}}_\Omega) - \chi_{\Omega 0} \text{sign}(\tilde{\mathbf{e}}_\Omega) - \dot{\Delta}_\Omega \end{cases} \quad (25)$$

According to the convergence analysis of the fixed-time non-recursive observer reported in [35], the error vector $\mathbf{e} = [\tilde{\mathbf{e}}_\Omega, \tilde{\Delta}_\Omega]^T$ is expected to converge to the origin in the fixed time. That is, the lumped disturbances Δ_Ω can be estimated within the fixed time $T_{\Omega 0}$. This completes the proof of Theorem 1.

3.1.3. Design of the QFFCL

This subsection describes the design of a novel QFFCL for the attitude angle subsystem to ensure the control performance.

First, based on the fixed-time theory, the non-singular fixed-time terminal sliding mode surface is intuitively designed as follows:

$$\boldsymbol{\sigma}_\Omega = \boldsymbol{\kappa}_\Omega + \int k_{\Omega c1} \text{sig}^{\alpha_{\Omega c1}}(\boldsymbol{\kappa}_\Omega) + k_{\Omega c2} \text{sig}^{\beta_{\Omega c1}}(\boldsymbol{\kappa}_\Omega) dt \quad (26)$$

where $\boldsymbol{\kappa}_\Omega = \mathbf{\Omega} - \mathbf{\Omega}_c = [\kappa_\alpha, \kappa_\beta, \kappa_\gamma]^T \in \mathbb{R}^{3 \times 1}$ represents the tracking error vector in the attitude angle loop and $k_{\Omega c1}, k_{\Omega c2} > 0$, $\alpha_{\Omega c1} \in (0, 1)$, and $\beta_{\Omega c1} > 1$ are the controller parameters.

Remark 1. According to (26), when $\dot{\boldsymbol{\sigma}}_\Omega = 0$,

$$\dot{\boldsymbol{\kappa}}_\Omega = -k_{\Omega c1} \text{sig}^{\alpha_{\Omega c1}}(\boldsymbol{\kappa}_\Omega) - k_{\Omega c2} \text{sig}^{\beta_{\Omega c1}}(\boldsymbol{\kappa}_\Omega) \quad (27)$$

According to Lemma 2, in the sliding phase, the tracking error $\boldsymbol{\kappa}_\Omega$ can converge within a fixed time, and the upper bound on the convergence time can be calculated as follows:

$$T_{\Omega c1} \leq \frac{1}{k_{\Omega c2}(\beta_{\Omega c1}-1)} + \frac{1}{k_{\Omega c1}(1-\alpha_{\Omega c1})} \quad (28)$$

Combining (17), (21), and (26), the QFFCL for the attitude angle subsystem can be designed as follows:

$$\tilde{\boldsymbol{\omega}} = -\mathbf{g}_\Omega^{-1} \left[\mathbf{f}_\Omega + \hat{\Delta}_\Omega - \dot{\mathbf{\Omega}}_c + \begin{pmatrix} k_{\Omega c1} \text{sig}^{\alpha_{\Omega c1}}(\boldsymbol{\kappa}_\Omega) + k_{\Omega c2} \text{sig}^{\beta_{\Omega c1}}(\boldsymbol{\kappa}_\Omega) \\ + k_{\Omega c3} \text{sig}^{\alpha_{\Omega c2}}(\boldsymbol{\sigma}_\Omega) + k_{\Omega c4} \text{sig}^{\beta_{\Omega c2}}(\boldsymbol{\sigma}_\Omega) \end{pmatrix} \right] \quad (29)$$

Remark 2. Focusing on the term \mathbf{g}_Ω in (8), it can be noted that $\det(\mathbf{g}_\Omega) = -\sec \beta$, and \mathbf{g}_Ω is irreversible when $\beta = \pm 90^\circ$. However, β is restricted to a neighborhood of zero in the reentry phase of the hypersonic vehicle. In other words, \mathbf{g}_Ω is reversible, and the control signal $\tilde{\omega}$ is non-singular.

3.2. Controller design for the angular rate subsystem

3.2.1. Design of the NFF

In the angular rate subsystem, the NFF is used to avoid the differential explosion problem. Similar to (20), the NFF is formulated as follows:

$$\tau_{\omega F} \dot{\omega}_c = -\text{sig}^{\alpha_{\omega F}}(\omega_c - \tilde{\omega}) - \text{sig}^{\beta_{\omega F}}(\omega_c - \tilde{\omega}) \tag{30}$$

where $\tilde{\omega}$ denotes the virtual reference command generated by the attitude angle control subsystem, ω_c represents the new virtual control input after filtering, $\dot{\omega}_c$ denotes the corresponding differential signal of ω_c ; $\tau_{\omega F}$ is a small positive constant, $\alpha_{\omega F} \in (0, 1)$, and $\beta_{\omega F} > 1$. The error of the NFF in the angular rate subsystem can be defined as $\epsilon_\omega = \omega_c - \tilde{\omega}$.

Remark 3. In this paper, the NFFs (20) and (30) are utilized to generate more realizable commands, generate the corresponding differential signals, and solve the differential explosion problem. The tuning rules for the parameters in the NFF are defined as follows: decreasing τ_i, α_i , and increasing $\beta_i (i = \Omega F, \omega F)$ accelerates the convergence and enhances the accuracy of the NFF. However, an excessively small τ_i, α_i and large β_i may render the NFF more sensitive to measurement noises and high-frequency dynamics, thereby affecting the stability of the system. Hence, the balance between the sensitivity and prompt responsiveness of the NFF should be considered in practical applications.

3.2.2. Design of the FESO

In the angular rate subsystem, the FESO is designed to estimate the lumped disturbances $\Delta_{\omega f}$ within a fixed time and is formulated as follows:

$$\begin{cases} \tilde{\mathbf{e}}_\omega = \hat{\omega} - \omega \\ \dot{\hat{\omega}} = \mathbf{f}_\omega + \mathbf{g}_\omega \mathbf{Q}(\mathbf{u}) - \mu_{\omega 01} \text{sig}^{\alpha_{\omega 01}}(\tilde{\mathbf{e}}_\omega) - \mu_{\omega 02} \text{sig}^{\beta_{\omega 01}}(\tilde{\mathbf{e}}_\omega) + \hat{\Delta}_{\omega f} \\ \dot{\hat{\Delta}}_{\omega f} = -\mu_{\omega 03} \text{sig}^{\alpha_{\omega 02}}(\tilde{\mathbf{e}}_\omega) - \mu_{\omega 04} \text{sig}^{\beta_{\omega 02}}(\tilde{\mathbf{e}}_\omega) - \chi_{\omega 0} \text{sign}(\tilde{\mathbf{e}}_\omega) \end{cases} \tag{31}$$

where $\hat{\omega}$ and $\hat{\Delta}_{\omega f}$ represent the estimates of the angular rate ω and lumped disturbances $\Delta_{\omega f}$ respectively; \mathbf{e}_ω denotes the estimation error; and $\alpha_{\omega 01} \in (0, 1)$, $\beta_{\omega 01} > 1$, $\alpha_{\omega 02} = 2\alpha_{\omega 01} - 1$, $\beta_{\omega 02} = 2\beta_{\omega 01} - 1$, $\chi_{\omega 0} > L_{\omega f}$, and $\mu_{\omega 0i} > 0 (i = 1, \dots, 4)$ are parameters to be designed.

According to Theorem 1, the lumped disturbances $\Delta_{\omega f}$ can be estimated within a fixed time by using the FESO, and the upper bound on the convergence time $T_{\omega 0}$ can be estimated as follows:

$$T_{\omega 0} \leq \frac{\lambda_{\max}(\Sigma_{\omega 1})^{(1-\alpha_{\omega 01})}}{\lambda_{\omega 1}(1-\alpha_{\omega 01})} + \frac{1}{\lambda_{\omega 2}(\beta_{\omega 01}-1)\varpi_\omega^{(\beta_{\omega 01}-1)}} \tag{32}$$

where $\lambda_{\omega 1} = \lambda_{\min}(Q_{\omega 1})/\lambda_{\max}(\Sigma_{\omega 1})$, $\lambda_{\omega 2} = \lambda_{\min}(Q_{\omega 2})/\lambda_{\max}(\Sigma_{\omega 2})$, $\lambda_{\min}(\Sigma_{\omega 2}) \geq \varpi_\omega > 0$, and $Q_{\omega 1}$, $\Sigma_{\omega 1}$, $Q_{\omega 2}$ and $\Sigma_{\omega 2}$ are positive definite matrices that satisfy

$$\begin{aligned} \Sigma_{\omega 1} P_{\omega 1} + P_{\omega 1}^T \Sigma_{\omega 1} &= -Q_{\omega 1}, \quad \Sigma_{\omega 2} P_{\omega 2} + P_{\omega 2}^T \Sigma_{\omega 2} = -Q_{\omega 2} \\ P_{\omega 1} &= \begin{bmatrix} -\mu_{\omega 01} & 1 \\ -\mu_{\omega 03} & 0 \end{bmatrix}, \quad P_{\omega 2} = \begin{bmatrix} -\mu_{\omega 02} & 1 \\ -\mu_{\omega 04} & 0 \end{bmatrix} \end{aligned} \tag{33}$$

Remark 4. The tuning rules for the FESO parameters defined in (21) and (31) can be described as follows: larger $\mu_{i1}, \mu_{i2}, \mu_{i3}, \mu_{i4}, \beta_{i1}, \beta_{i2}$ and smaller $\alpha_{i1}, \alpha_{i2} (i = \Omega 0, \omega 0)$ accelerate the convergence. However, an excessively large $\mu_{i1}, \mu_{i2}, \mu_{i3}, \mu_{i4}, \beta_{i1}, \beta_{i2}$ and small α_{i1}, α_{i2} may lead to a large overshoot. Hence, the balance between the overshoot and prompt responsiveness of the FESO should be considered in practical applications.

3.2.3. Design of the QFFCL

Similar to the attitude angle subsystem, the sliding mode surface of the angular rate subsystem can be designed as follows:

$$\sigma_\omega = \kappa_\omega + \int k_{\omega c1} \text{sig}^{\alpha_{\omega c1}}(\kappa_\omega) + k_{\omega c2} \text{sig}^{\beta_{\omega c1}}(\kappa_\omega) dt \tag{34}$$

where $\kappa_\omega = \omega - \omega_c = [\kappa_{\omega x}, \kappa_{\omega y}, \kappa_{\omega z}]^T \in \mathbb{R}^{3 \times 1}$ represents the tracking error vector in the angular rate loop and $k_{\omega c1}, k_{\omega c2} > 0$, $\alpha_{\omega c1} \in (0, 1)$, $\beta_{\omega c1} > 1$ are the controller parameters.

According to Lemma 2 and Remark 1, when $\dot{\sigma}_\omega = 0$,

$$\dot{\kappa}_\omega = -k_{\omega c1} \text{sig}^{\alpha_{\omega c1}}(\kappa_\omega) - k_{\omega c2} \text{sig}^{\beta_{\omega c1}}(\kappa_\omega) \tag{35}$$

Algorithm 1
Implementation Framework of the Proposed Control Scheme.

-
- 1: Initialize NFFs ((20) and (30)), FESOs ((21) and (31)), QFFCLs ((29) and (37)), and HQ (13).
 - 2: At each sampling time $t_i, i = 0, 1, \dots$
 - 3: (1) Obtain the current desired command $\tilde{\omega}$ and HRV states Ω, ω .
 - 4: (2) Acquire the filtered command Ω_c and differential signal $\tilde{\Omega}_c$ by using (20).
 - 5: (3) Obtain the estimation of the lumped disturbances $\hat{\Delta}_\Omega$ by using (21).
 - 6: (4) Calculate the tracking error κ_Ω and obtain the virtual angular rate command $\tilde{\omega}$ by using (29).
 - 7: (5) Obtain the filtered command ω_c and differential signal $\tilde{\omega}_c$ by using (30).
 - 8: (6) Get the estimate of the lumped disturbances $\hat{\Delta}_{\omega_f}$ by using (31).
 - 9: (7) Calculate the tracking error κ_ω and obtain the desired control instruction u_c by using (37).
 - 10: (8) The HQ module determines whether the control inputs must be updated using (13) and returns to step (1).
-

The tracking error κ_ω can converge within a fixed time, and the upper bound of the convergence time can be calculated as follows:

$$T_{\omega c1} \leq \frac{1}{k_{\omega c2}(\beta_{\omega c1} - 1)} + \frac{1}{k_{\omega c1}(1 - \alpha_{\omega c1})} \tag{36}$$

Based on the quantization decomposition technique expressed in (14) and in combination with (17), (31), and (34), the QFFCL for the angular rate subsystem can be designed as follows:

$$u_c = -\tau_\omega \cdot g_\omega^{-1} \left[\begin{array}{l} f_\omega + \hat{\Delta}_{\omega_f} - \dot{\omega}_c \\ + \left(k_{\omega c1} \text{sig}^{\alpha_{\omega c1}}(\kappa_\omega) + k_{\omega c2} \text{sig}^{\beta_{\omega c1}}(\kappa_\omega) \right) \\ + \left(k_{\omega c3} \text{sig}^{\alpha_{\omega c2}}(\sigma_\omega) + k_{\omega c4} \text{sig}^{\beta_{\omega c2}}(\sigma_\omega) \right) \end{array} \right] \tag{37}$$

where $\tau_\omega = \text{diag}\{1/(1 - \tau_e), 1/(1 - \tau_a), 1/(1 - \tau_r)\}$.

Remark 5. In this paper, the QFFCLs (29) and (37) are adopted to ensure that the system converges within a fixed time. The exponential coefficients β_{i1} and $\beta_{i2}(i = \Omega c, \omega c)$ drive the system to converge rapidly when the state is far from the origin, and the exponential coefficients α_{i1} and $\alpha_{i2}(i = \Omega c, \omega c)$ drive the system to converge rapidly when the state is close to the origin. The tuning rules for the parameters in the QFFCL can be defined as follows: larger $k_{i1}, k_{i2}, k_{i3}, k_{i4}, \beta_{i1}, \beta_{i2}$ and smaller α_{i1}, α_{i2} accelerate the convergence and reduce the steady system error. However, an excessively large $k_{i1}, k_{i2}, k_{i3}, k_{i4}, \beta_{i1}, \beta_{i2}$ and small α_{i1}, α_{i2} may lead to a large control input, which may exceed the actual physical constraints of the HRV. Hence, the tradeoff between the control effort and prompt responsiveness of the QFFCL must be considered in practical applications.

The abovementioned sections described the design process of the proposed controller. For convenient expression, the detailed implementation procedure of the proposed control scheme is summarized as the pseudocode Algorithm 1.

3.3. Stability analysis

Lemma 3. [36]: Considering the universal nonlinear system $\dot{x} = f(x(t)), x(0) = x_0$, if there exists a continuous positive definite and radially unbounded Lyapunov function $V(x): \mathbb{R}^n \times 1 \rightarrow \mathbb{R}$ and parameters m_1, m_2, p_1, p_2 , and Δ_V satisfying $m_1, m_2 > 0, p_1 > 1, 0 < p_2 < 1, 0 < \Delta_V < \infty$, if $\dot{V}(x) \leq -m_1 V(x)^{p_1} - m_2 V(x)^{p_2} + \Delta_V$, then the system is considered to be practical fixed-time stable, and the residual set of the trajectory Θ and settling time T can be defined as

$$\Theta = \left\{ \lim_{t \rightarrow T} x | V(x) \leq \min \left[\left(\frac{\Delta_V}{m_1(1-\theta)} \right)^{\frac{1}{p_1}}, \left(\frac{\Delta_V}{m_2(1-\theta)} \right)^{\frac{1}{p_2}} \right] \right\}$$

$$T \leq \frac{1}{m_1 \theta (p_1 - 1)} + \frac{1}{m_2 \theta (1 - p_2)} \tag{38}$$

where $0 < \theta < 1$.

Lemma 4. [37]: For $x_i \in \mathbb{R}, i = 1, 2, \dots, N, q_1 > 1, 0 < q_2 < 1$, then

$$\left(\sum_{i=1}^N |x_i| \right)^{q_1} \leq N^{q_1-1} \sum_{i=1}^N |x_i|^{q_1}$$

$$\left(\sum_{i=1}^N |x_i| \right)^{q_2} \leq \sum_{i=1}^N |x_i|^{q_2} \tag{39}$$

Theorem 2. Suppose that Assumption 1 is valid. If the HRV attitude control system is described by (17), the HQ is described by (13), the FESOs are described by (21) and (31), and the QFFCLs are described by (29) and (37), the closed-loop system is practical fixed-time stable, and the sliding mode σ_i and tracking error $\kappa_i(i = \Omega, \omega)$ converge into the small regions in the fixed time.

Proof. The Lyapunov function is selected as follows:

$$V = \frac{1}{2} \sigma_\Omega^T \sigma_\Omega + \frac{1}{2} \sigma_\omega^T \sigma_\omega + \frac{1}{2} \epsilon_\Omega^T \epsilon_\Omega + \frac{1}{2} \epsilon_\omega^T \epsilon_\omega + \frac{1}{2} \tilde{\Delta}_\Omega^T \tilde{\Delta}_\Omega + \frac{1}{2} \tilde{\Delta}_{\omega_f}^T \tilde{\Delta}_{\omega_f} \tag{40}$$

The time derivative of V is

$$\dot{V} = \sigma_{\Omega}^T \dot{\sigma}_{\Omega} + \sigma_{\omega}^T \dot{\sigma}_{\omega} + \epsilon_{\Omega}^T \dot{\epsilon}_{\Omega} + \epsilon_{\omega}^T \dot{\epsilon}_{\omega} + \tilde{\Delta}_{\Omega}^T \dot{\tilde{\Delta}}_{\Omega} + \tilde{\Delta}_{\omega}^T \dot{\tilde{\Delta}}_{\omega} \tag{41}$$

First, recalling [Theorem 1](#), when $t > T_0 = \max(T_{\Omega_0}, T_{\omega_0})$, $\tilde{\Delta}_{\Omega} = 0$, $\tilde{\Delta}_{\omega} = 0$. Then, based on the definitions of ϵ_{Ω} and ϵ_{ω} , one can obtain that

$$\dot{\epsilon}_{\Omega} = -\frac{\text{sig}^{\alpha_{\Omega F}}(\epsilon_{\Omega})}{\tau_{\Omega F}} - \frac{\text{sig}^{\beta_{\Omega F}}(\epsilon_{\Omega})}{\tau_{\Omega F}} - \dot{\tilde{\omega}}, \dot{\epsilon}_{\omega} = -\frac{\text{sig}^{\alpha_{\omega F}}(\epsilon_{\omega})}{\tau_{\omega F}} - \frac{\text{sig}^{\beta_{\omega F}}(\epsilon_{\omega})}{\tau_{\omega F}} - \dot{\tilde{\omega}} \tag{42}$$

In practical engineering scenarios, the command signal $\tilde{\omega}$ is given by the guidance algorithm in which the first-order derivative of $\tilde{\omega}$ is bounded, such that $\|\dot{\tilde{\omega}}\| \leq \zeta_{\Omega}$ with a positive constant ζ_{Ω} . According to [\(29\)](#) and [Remark 2](#), it turns out that the first-order derivative of $\tilde{\omega}$ is also bounded, such that $\|\dot{\tilde{\omega}}\| \leq \zeta_{\omega}$ with a positive constant ζ_{ω} . Hence, we can get

$$\dot{\epsilon}_{\Omega} \leq -\frac{\text{sig}^{\alpha_{\Omega F}}(\epsilon_{\Omega})}{\tau_{\Omega F}} - \frac{\text{sig}^{\beta_{\Omega F}}(\epsilon_{\Omega})}{\tau_{\Omega F}} + \mathbf{v}_{\Omega}, \dot{\epsilon}_{\omega} \leq -\frac{\text{sig}^{\alpha_{\omega F}}(\epsilon_{\omega})}{\tau_{\omega F}} - \frac{\text{sig}^{\beta_{\omega F}}(\epsilon_{\omega})}{\tau_{\omega F}} + \mathbf{v}_{\omega} \tag{43}$$

where $\mathbf{v}_{\Omega} = [\zeta_{\Omega} \zeta_{\Omega} \zeta_{\Omega}]^T$, $\mathbf{v}_{\omega} = [\zeta_{\omega} \zeta_{\omega} \zeta_{\omega}]^T$.

Then, recalling [Lemma 1](#), substituting [\(29\)](#), [\(37\)](#), and [\(43\)](#) into [\(41\)](#) yields

$$\begin{aligned} \dot{V} \leq & \sigma_{\Omega}^T \left[-k_{\Omega c3} \text{sig}^{\alpha_{\Omega c2}}(\sigma_{\Omega}) - k_{\Omega c4} \text{sig}^{\beta_{\Omega c2}}(\sigma_{\Omega}) \right] + \sigma_{\omega}^T \left[-k_{\omega c3} \text{sig}^{\alpha_{\omega c2}}(\sigma_{\omega}) - k_{\omega c4} \text{sig}^{\beta_{\omega c2}}(\sigma_{\omega}) \right] \\ & + \epsilon_{\Omega}^T \left(-\frac{\text{sig}^{\alpha_{\Omega F}}(\epsilon_{\Omega})}{\tau_{\Omega F}} - \frac{\text{sig}^{\beta_{\Omega F}}(\epsilon_{\Omega})}{\tau_{\Omega F}} + \mathbf{v}_{\Omega} \right) + \epsilon_{\omega}^T \left(-\frac{\text{sig}^{\alpha_{\omega F}}(\epsilon_{\omega})}{\tau_{\omega F}} - \frac{\text{sig}^{\beta_{\omega F}}(\epsilon_{\omega})}{\tau_{\omega F}} + \mathbf{v}_{\omega} \right) \end{aligned} \tag{44}$$

Using Young's inequality, the following expression can be derived:

$$\epsilon_{\Omega}^T \mathbf{v}_{\Omega} \leq \frac{\epsilon_{\Omega}^T \epsilon_{\Omega}}{2} + \frac{\mathbf{v}_{\Omega}^T \mathbf{v}_{\Omega}}{2}, \epsilon_{\omega}^T \mathbf{v}_{\omega} \leq \frac{\epsilon_{\omega}^T \epsilon_{\omega}}{2} + \frac{\mathbf{v}_{\omega}^T \mathbf{v}_{\omega}}{2} \tag{45}$$

Setting $\alpha_F = \alpha_{\Omega F} = \alpha_{\omega F}$, $\beta_F = \beta_{\Omega F} = \beta_{\omega F}$, and $\tau = \tau_{\Omega F} = \tau_{\omega F}$, invoking [\(45\)](#) in [\(44\)](#) and merging the right side of [\(44\)](#) yields

$$\begin{aligned} \dot{V} \leq & -k_{\Omega c3} (\sigma_{\Omega}^T \sigma_{\Omega})^{\frac{\alpha_{\Omega c2}+1}{2}} - k_{\Omega c4} (\sigma_{\Omega}^T \sigma_{\Omega})^{\frac{\beta_{\Omega c2}+1}{2}} - k_{\omega c3} (\sigma_{\omega}^T \sigma_{\omega})^{\frac{\alpha_{\omega c2}+1}{2}} - k_{\omega c4} (\sigma_{\omega}^T \sigma_{\omega})^{\frac{\beta_{\omega c2}+1}{2}} \\ & - \left(\frac{1}{\tau} - 1\right) (\epsilon_{\Omega}^T \epsilon_{\Omega})^{\frac{\alpha_F+1}{2}} - \left(\frac{1}{\tau} - 1\right) (\epsilon_{\Omega}^T \epsilon_{\Omega})^{\frac{\beta_F+1}{2}} - \left(\frac{1}{\tau} - 1\right) (\epsilon_{\omega}^T \epsilon_{\omega})^{\frac{\alpha_F+1}{2}} - \left(\frac{1}{\tau} - 1\right) (\epsilon_{\omega}^T \epsilon_{\omega})^{\frac{\beta_F+1}{2}} \\ & + \frac{\mathbf{v}_{\Omega}^T \mathbf{v}_{\Omega}}{2} + \frac{\mathbf{v}_{\omega}^T \mathbf{v}_{\omega}}{2} \end{aligned} \tag{46}$$

Setting $\alpha_F = \alpha_{ic2} = \alpha_{c2}$ and $\beta_F = \beta_{ic2} = \beta_{c2}$ ($i = \Omega, \omega$) yields

$$\begin{aligned} \dot{V} \leq & -A_1 \left[(\sigma_{\Omega}^T \sigma_{\Omega})^{\frac{\alpha_{c2}+1}{2}} + (\sigma_{\omega}^T \sigma_{\omega})^{\frac{\alpha_{c2}+1}{2}} \right] - A_2 \left[(\sigma_{\Omega}^T \sigma_{\Omega})^{\frac{\beta_{c2}+1}{2}} + (\sigma_{\omega}^T \sigma_{\omega})^{\frac{\beta_{c2}+1}{2}} \right] \\ & - A_3 \left[(\epsilon_{\Omega}^T \epsilon_{\Omega})^{\frac{\alpha_{c2}+1}{2}} + (\epsilon_{\omega}^T \epsilon_{\omega})^{\frac{\alpha_{c2}+1}{2}} \right] - A_3 \left[(\epsilon_{\Omega}^T \epsilon_{\Omega})^{\frac{\beta_{c2}+1}{2}} + (\epsilon_{\omega}^T \epsilon_{\omega})^{\frac{\beta_{c2}+1}{2}} \right] \\ & + \frac{\mathbf{v}_{\Omega}^T \mathbf{v}_{\Omega}}{2} + \frac{\mathbf{v}_{\omega}^T \mathbf{v}_{\omega}}{2} \end{aligned} \tag{47}$$

where $A_1 = \min(k_{\Omega c3}, k_{\omega c3})$, $A_2 = \min(k_{\Omega c4}, k_{\omega c4})$, and $A_3 = 1/\tau - 1$.

Then, using [Lemma 4](#), we can obtain

$$\begin{aligned} \dot{V} \leq & -A_1 (\sigma_{\Omega}^T \sigma_{\Omega} + \sigma_{\omega}^T \sigma_{\omega})^{\frac{\alpha_{c2}+1}{2}} - 2^{\frac{1-\beta_{c2}}{2}} A_2 (\sigma_{\Omega}^T \sigma_{\Omega} + \sigma_{\omega}^T \sigma_{\omega})^{\frac{\beta_{c2}+1}{2}} \\ & - A_3 (\epsilon_{\Omega}^T \epsilon_{\Omega} + \epsilon_{\omega}^T \epsilon_{\omega})^{\frac{\alpha_{c2}+1}{2}} - 2^{\frac{1-\beta_{c2}}{2}} A_3 (\epsilon_{\Omega}^T \epsilon_{\Omega} + \epsilon_{\omega}^T \epsilon_{\omega})^{\frac{\beta_{c2}+1}{2}} + \frac{\mathbf{v}_{\Omega}^T \mathbf{v}_{\Omega}}{2} + \frac{\mathbf{v}_{\omega}^T \mathbf{v}_{\omega}}{2} \\ \leq & -B_1 (\sigma_{\Omega}^T \sigma_{\Omega} + \sigma_{\omega}^T \sigma_{\omega} + \epsilon_{\Omega}^T \epsilon_{\Omega} + \epsilon_{\omega}^T \epsilon_{\omega})^{\frac{\alpha_{c2}+1}{2}} - B_2 (\sigma_{\Omega}^T \sigma_{\Omega} + \sigma_{\omega}^T \sigma_{\omega} + \epsilon_{\Omega}^T \epsilon_{\Omega} + \epsilon_{\omega}^T \epsilon_{\omega})^{\frac{\beta_{c2}+1}{2}} \\ & + \frac{\mathbf{v}_{\Omega}^T \mathbf{v}_{\Omega}}{2} + \frac{\mathbf{v}_{\omega}^T \mathbf{v}_{\omega}}{2} \\ \leq & -C_1 V^{\frac{\alpha_{c2}+1}{2}} - C_2 V^{\frac{\beta_{c2}+1}{2}} + \Delta_V \end{aligned} \tag{48}$$

where $B_1 = \min(A_1, A_3)$, $B_2 = \min(2^{\frac{1-\beta_{c2}}{2}} A_2, 2^{\frac{1-\beta_{c2}}{2}} A_3) 2^{\frac{1-\beta_{c2}}{2}}$, $C_1 = 2^{\frac{\alpha_{c2}+1}{2}} \min(k_{\Omega c3}, k_{\omega c3})$, $C_2 = 2 \min(2^{\frac{\beta_{c2}-1}{2}} A_2, 2^{\frac{\beta_{c2}-1}{2}} A_3)$, and $\Delta_V = (\mathbf{v}_{\Omega}^T \mathbf{v}_{\Omega} + \mathbf{v}_{\omega}^T \mathbf{v}_{\omega})/2$.

According to [Lemma 3](#), we can obtain that the system is fixed-time stable. Furthermore, the residual set of the trajectory Θ_{σ} and settling time T_{σ} can be given by $\Theta_{\sigma} = \{\lim_{t \rightarrow T_{\sigma}} |V(x)| \leq \min([\Delta_V / (C_1(1-\theta))]^{2/(\alpha_{c2}+1)}, [\Delta_V / (C_2(1-\theta))]^{2/(\beta_{c2}+1)})\}$, $T_{\sigma} \leq 1/(m_1 \theta ((\alpha_{c2} - 1)/2)) + 1/(m_2 \theta ((\beta_{c2} - 1)/2))$. Thus, the proof of [Theorem 2](#) is complete.

4. Simulation and discussion

In this section, comparative simulation and Monte Carlo simulation are performed to verify the effectiveness, superiority, and robustness of the proposed control scheme. The geometrical configuration and parameters of the HRV are shown in [Fig. 2](#) and listed in [Table 1](#), respectively.

Table 2
Controller parameters.

Module	Parameters
NFF Eqs. (20) and ((30))	$\tau_i = 0.1, \alpha_i = 0.8, \beta_i = 1.2(i = \Omega F, \omega F)$ $\alpha_{i01} = 0.8, \beta_{i01} = 1.2(i = \Omega, \omega)$
FESO Eqs. (21) and ((31))	$\mu_{\Omega\omega 1} = \mu_{\Omega\omega 3} = 10, \mu_{\Omega\omega 2} = \mu_{\Omega\omega 4} = 50, \chi_s = 50$ $\mu_{\omega\omega 1} = \mu_{\omega\omega 3} = 10, \mu_{\omega\omega 2} = \mu_{\omega\omega 4} = 20, \chi_\omega = 100$
HQ (Eqs. (13))	$\rho_m = 0.95, \delta_{m,\min} = 0.3(m = e, a, r)$ $\alpha_{e2} = 0.8, \beta_{e2} = 1.2$
QFFCL Eqs. (29) and (37)	$k_{\Omega c1} = 0.6, k_{\Omega c2} = 0.9, k_{\Omega c3} = 0.5, k_{\Omega c4} = 0.5$ $k_{\omega c1} = 2, k_{\omega c2} = 4, k_{\omega c3} = 0.5, k_{\omega c4} = 0.9$
HOSMO-ADRC [38]	$C_{11} = C_{12} = C_{13} = 0.05, C_{21} = C_{22} = C_{23} = 0.8$ $k_{is} = 0.56, k_{ps} = 1.5, k_{if} = 2.25, k_{pf} = 3$ $l_1 = 0.5, l_2 = 0.15, l_3 = 0.1, p = 1.5$
Finite-time SMC [21]	$l_4 = 1.6, l_5 = 0.15, l_6 = 1.2$
ESO [32]	$k_1 = 1.2, k_2 = 1.5, r_1 = 0.4, r_2 = 0.8$ $\mathbf{w}_{\omega 1} = 25\mathbf{I}_3, \mathbf{w} = 50\mathbf{I}_3$

4.1. Comparative simulation

In this subsection, to reveal the effectiveness and superiority of the proposed controller, the high order sliding mode observer-based active disturbance rejection control (HOSMO-ADRC) fault-tolerant scheme [38] and finite-time sliding mode control (Finite-time SMC) fault-tolerant scheme [21] are considered to perform the comparative analysis. Moreover, the ESO [32] and the HOSMO [38] are adopted to demonstrate the efficacy of the FESO.

The initial conditions of the HRV are as follows: $H = 52.1\text{km}, V = 3608\text{m/s}, \alpha = \beta = \gamma_s = 0.1^\circ$, and $w_x = w_y = w_z = 0.1^\circ/\text{s}$. The controller parameters are given in Table 2. The aerodynamic coefficients deviate from the nominal value by +20%, that is, $\Delta_F = \Delta_M = 20\%$. The external disturbances are formulated as follows:

$$\mathbf{d}_\Omega = \begin{bmatrix} 0.01 + 0.01\sin(0.2t)\cos(0.3t) - 0.01\sin(0.2t)\exp(-0.02t) \\ 0.01 - 0.01\sin(0.3t)\cos(0.2t) + 0.01\sin(0.2t)\exp(-0.02t) \\ 0.01 + 0.01\sin(0.2t)\cos(0.3t) - 0.01\sin(0.2t)\exp(-0.02t) \end{bmatrix} \tag{49}$$

$$\mathbf{d}_\omega = 2\mathbf{d}_\Omega$$

where $\mathbf{d}_\Omega = [d_\alpha, d_\beta, d_{\gamma_s}]^T, \mathbf{d}_\omega = [d_{w_x}, d_{w_y}, d_{w_z}]^T$.

The actuator faults are set as follows:

$$\lambda_e = \begin{cases} 1 & t \leq 10 \\ 1 - 0.1 \cdot (t - 10) & 10 < t \leq 14, \zeta_e = \begin{cases} 0^\circ & t \leq 24 \\ 1^\circ & t > 24 \end{cases} \\ 0.6t & t > 14 \end{cases}$$

$$\lambda_a = \begin{cases} 1 & t \leq 14 \\ 1 - 0.1 \cdot (t - 14) & 14 < t \leq 18, \zeta_a = \begin{cases} 0^\circ & t \leq 24 \\ -1^\circ & t > 24 \end{cases} \\ 0.6t & t > 18 \end{cases} \tag{50}$$

$$\lambda_r = \begin{cases} 1 & t \leq 18 \\ 1 - 0.1 \cdot (t - 18) & 18 < t \leq 22, \zeta_r = \begin{cases} 0^\circ & t \leq 24 \\ 1^\circ & t > 24 \end{cases} \\ 0.6t & t > 22 \end{cases}$$

The comparison curves of the attitude angle tracking performance and tracking error are shown in Figs. 4 and 5. It is not difficult to find from Fig. 4 that the attitude angle subsystem exhibits a higher convergence speed and tracking accuracy when using the proposed controller, compared to those when using the HOSMO-ADRC and Finite-time SMC scheme. Especially, as can be seen from Fig. 5, when the bias faults $\zeta_i(i = e, a, r)$ occur at $t = 24\text{s}$, significant tracking error appears in the attitude angle subsystem. The proposed FTC scheme can accomplish attitude tracking more effectively and rapidly than the two existing FTC schemes.

Figs. 6 and 7 show the comparison curves of the angular rate tracking performance and tracking error. It is also interesting to observe from Figs. 6 and 7 that the proposed controller demonstrates a superior control performance even in the presence of uncertainties, external disturbances, and actuator faults compared with the two FTC schemes.

The mean absolute error (Mean-AE) and max absolute error (Max-AE) indexes presented in Table 3 are considered to evaluate the control performances of the three control methods more clearly and quantitatively. The Mean-AE and Max-AE indexes of the proposed controller are smaller than those of the other two methods. Hence, the proposed controller exhibits a higher steady-state control performance and transient control performance than the other two methods.

Figs. 8 and 9 show the comparison of the estimation performance of the ESO, HOSMO, and FESO in the attitude angle subsystem and angular rate subsystem, respectively. It is evident that compared with the asymptotic-convergent ESO and finite-time-convergent HOSMO, the proposed FESO exhibits a higher estimation performance under the application of the fixed-time convergence theory. That is, the FESO can compensate for the negative effect of actuator faults, uncertainties, and external disturbances within the allowable time for recovery from a fault scenario.

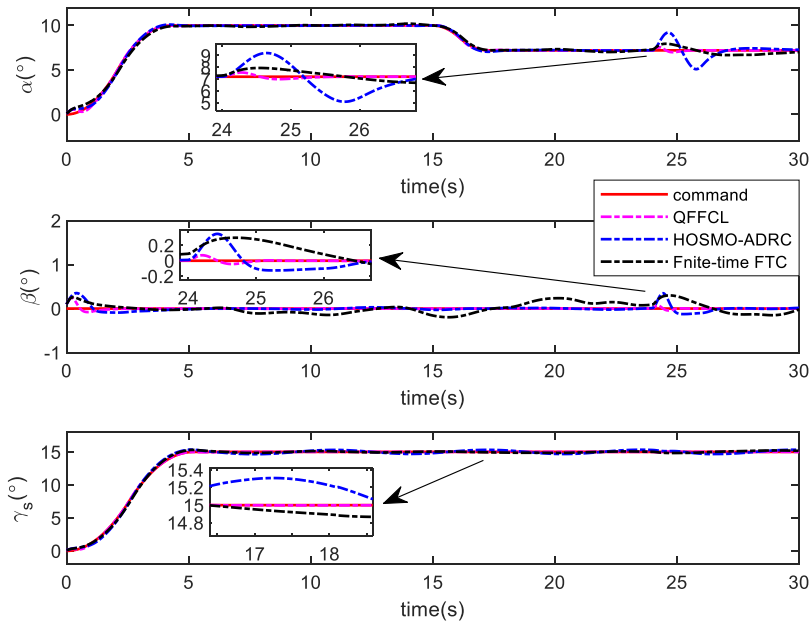


Fig. 4. Comparison curves of the attitude angle tracking performance.

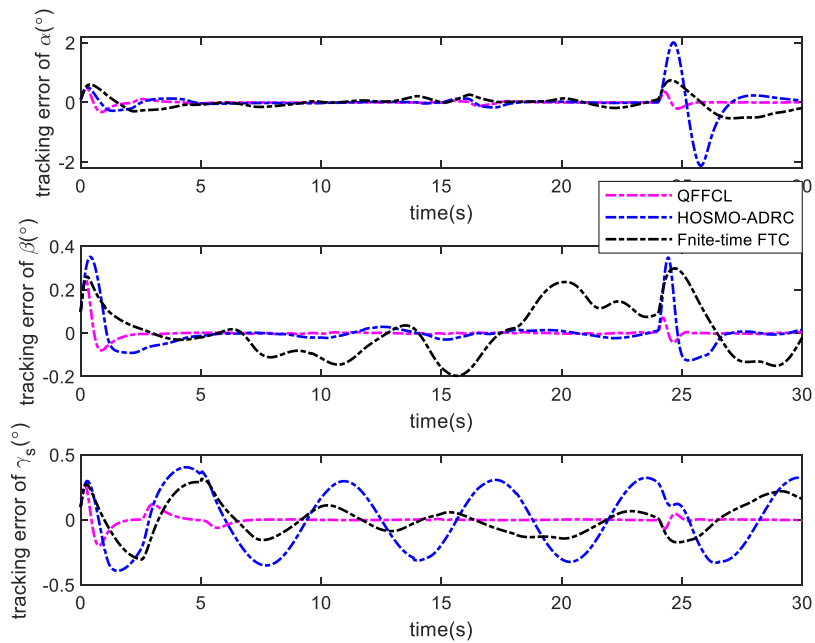


Fig. 5. Comparison curves of attitude angle tracking error.

Table 3
Comparison of control performance indexes of three control methods.

Index	Channel	QFFCL	HOSMO-ADRC	Finite-time SMC
Mean-AE	α	0.0324	0.1721	0.1672
	β	0.0080	0.0342	0.1002
	γ_s	0.0149	0.2171	0.1073
	Total	0.0553	0.4234	0.3747
Max-AE	α	0.5002	2.1185	0.7424
	β	0.2476	0.3519	0.2986
	γ_s	0.2603	0.4041	0.3161
	Total	1.0081	2.8745	1.3571

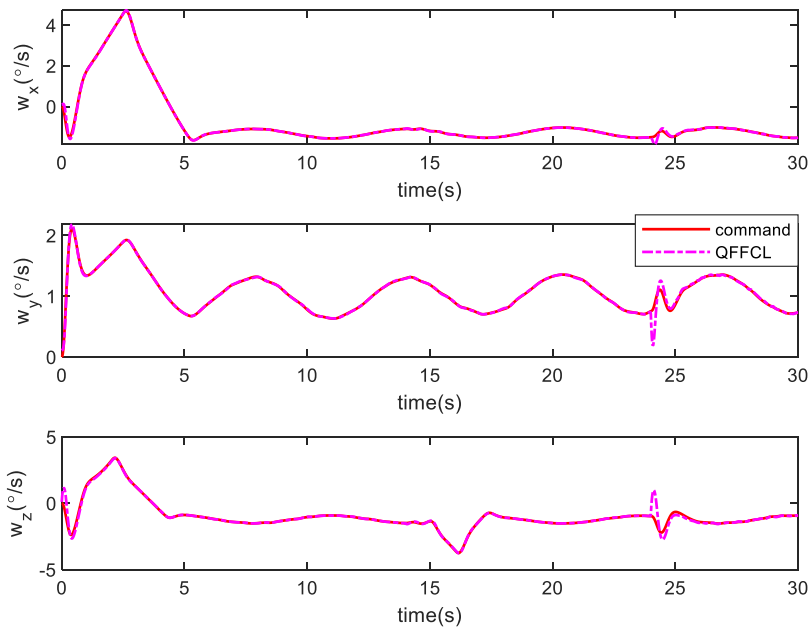


Fig. 6. Comparison curves of the angular rate tracking performance.

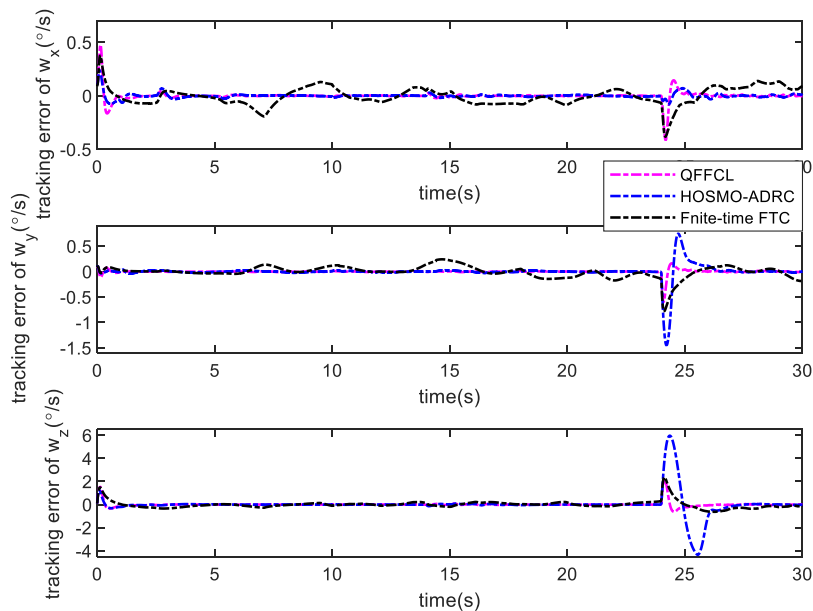


Fig. 7. Comparison curves of angular rate tracking error.

The curves of the response and number of communication events of the actuators are shown in Figs. 10–12. It can be noted that the HQ reduces the communication load by changing the continuous control signals into discrete quantized signals. Considering the $\delta_r - time$ curve in Fig. 12 as an example, when the time t ranges from 19.7 to 20.1 s, as shown by the red dotted line, the control signal without the HQ needs to be transmitted to the actuator module in real time within each control cycle. However, as shown by the blue dotted line, under the effect of the HQ, the continuous control signal is divided into a segmented control signal. In other words, the control signal needs to be transmitted to the actuator module only when the segmented control signal changes, thereby effectively reducing the number of communication events, which makes the proposed approach more suitable for situations in which the communication bandwidth and resources are limited. Similarly, the HQ significantly reduces the communication times and load, as indicated by the curves of the number of communication events.

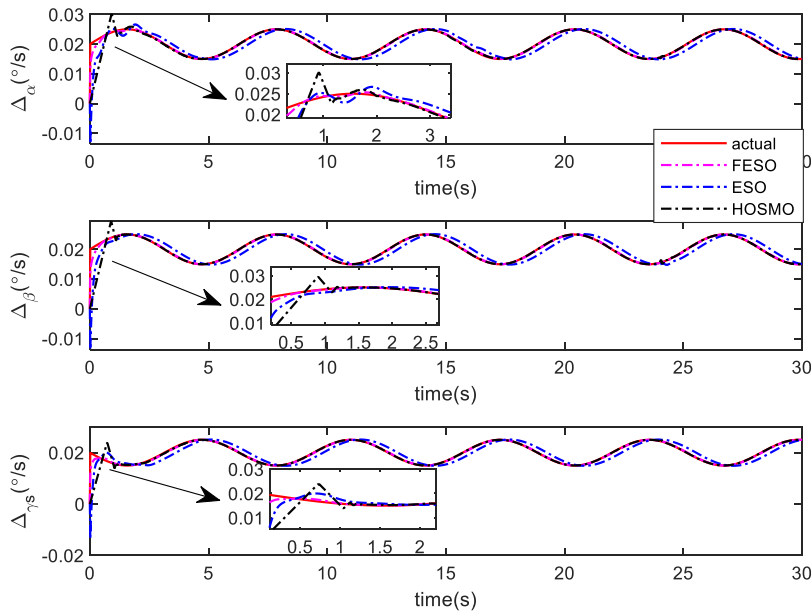


Fig. 8. Observer estimated curves of Δ_{Ω} .

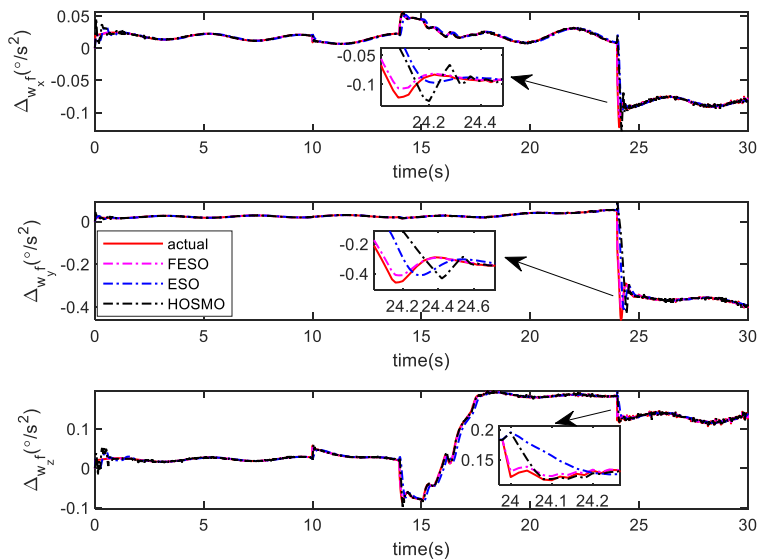


Fig. 9. Observer estimated curves of Δ_{ω_f} .

The comparison of the Mean-AE index and communication time of the QFFCL with and without the HQ is presented in Table 4. It can be quantitatively found that the number of communication events reduces by 35.93% under the effect of the HQ; meanwhile, under the effect of the proposed QFFCL, the total Mean-AE index increases by not even 2.79%. Therefore, the existence of the HQ in the proposed control scheme can effectively reduce the communication load with a finite loss in tracking accuracy.

4.2. Monte Carlo simulation

As described in this subsection, Monte Carlo simulations involving 300 iterations are performed to illustrate the robustness of the proposed QFFCL against aerodynamic coefficient perturbations, external disturbances, different initial conditions for the attitude angle, and angular rate, and actuator faults.

The initial conditions for the height and velocity of the HRV are $H = 52.1\text{km}$, $V = 3608\text{m/s}$, respectively.

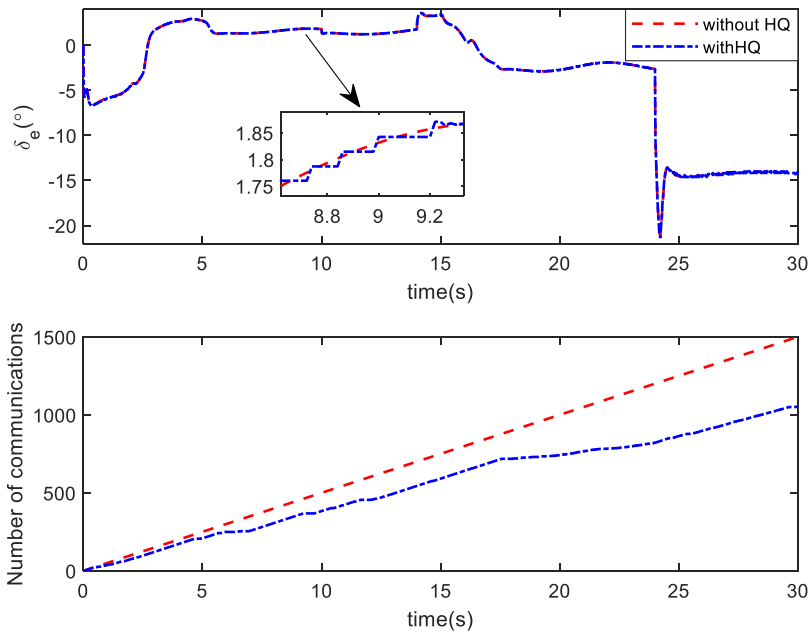


Fig. 10. Curves of the response and number of communication events of δ_e .

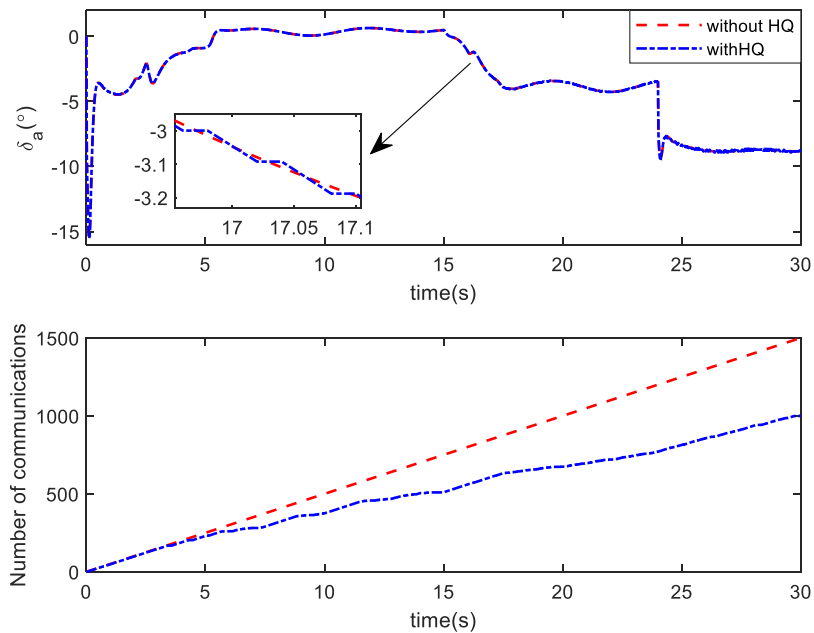


Fig. 11. Curves of the response and number of communication events of δ_a .

Table 4
Comparison of Mean-AE and communication times of QFFCL with and without the HQ.

Index	Channel	QFFCL (with HQ)	QFFCL (without HQ)	Increment (%)
Mean-AE	α	0.0324	0.0317	+2.21
	β	0.0080	0.0077	+2.60
	γ_s	0.0149	0.0144	+3.47
	Total	0.0553	0.0538	+2.79
Number of communication events	δ_e	1049	1500	-30.07
	δ_a	1011	1500	-32.60
	δ_r	823	1500	-45.13
	Total	2883	4500	-35.93

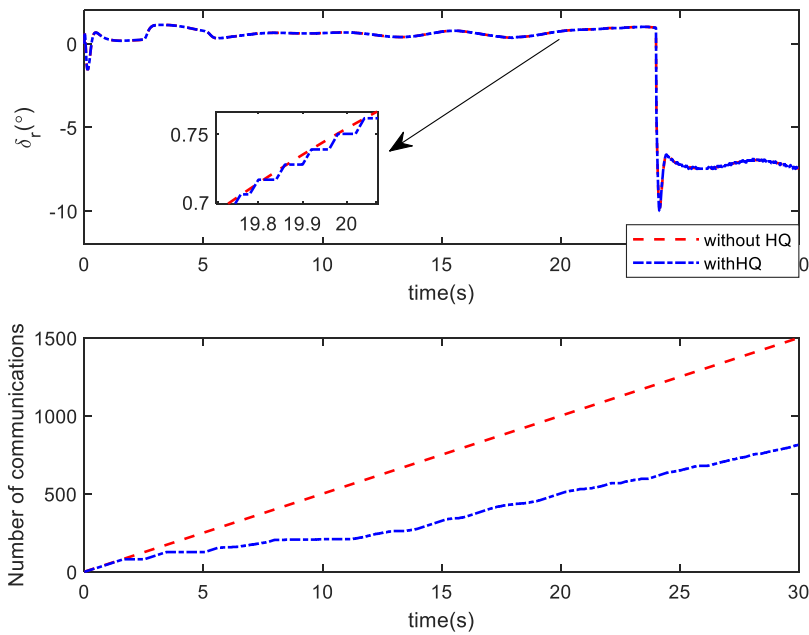


Fig. 12. Curves of the response and number of communication events of δ_r .

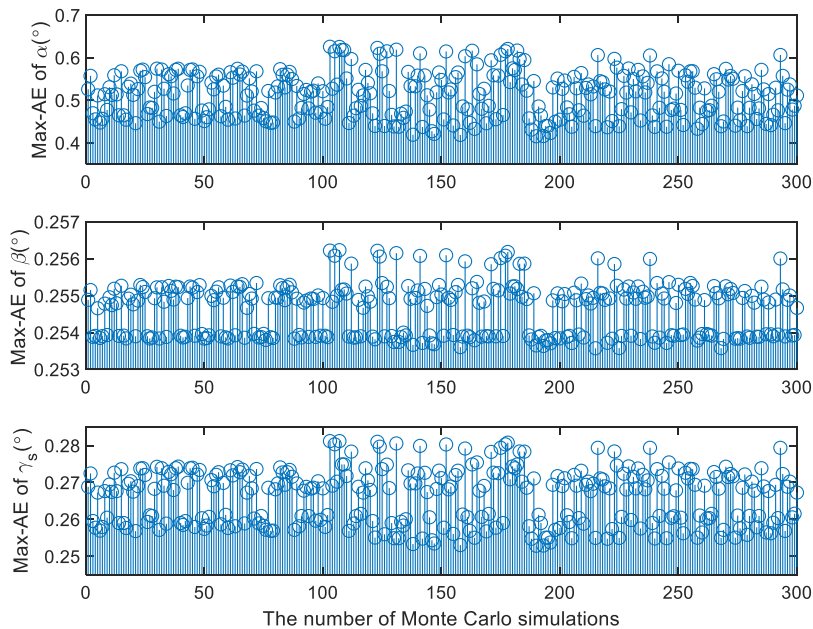


Fig. 13. Statistical charts of the Max-AE index for the Monte Carlo results.

The initial value ranges for the attitude angle Ω and angular rate ω are set as $[0^\circ, 0.3^\circ]$ and $[0^\circ/s, 0.3^\circ/s]$, respectively. The range of aerodynamic coefficient perturbations Δ_F and Δ_M are set as $[-20\%, +20\%]$. The external disturbances \mathbf{d}_Ω and \mathbf{d}_ω are formulated as indicated in (41). The ranges of λ_i and ζ_i ($i = e, a, r$) are set as $[0.6, 1]$ and $[-1^\circ, 1^\circ]$, respectively. In the Monte Carlo simulation, the relevant state initial values, coefficient perturbations, and fault parameters are randomly selected in the abovementioned ranges.

To more clearly illustrate the Monte Carlo results, the Mean-AE and Max-AE indexes of the attitude angle in 300 runs of the Monte Carlo simulations are shown in Figs. 13 and 14. It can be found that the attitude angle can track the command signal with a high tracking performance when driven by the proposed controller. In Table 5, by comparing the integer average of the number of communication events in the controller-to-actuator channel of the results of 300 runs of Monte Carlo simulations, it can be observed that the number of communication events is reduced by 31.62% under the effect of

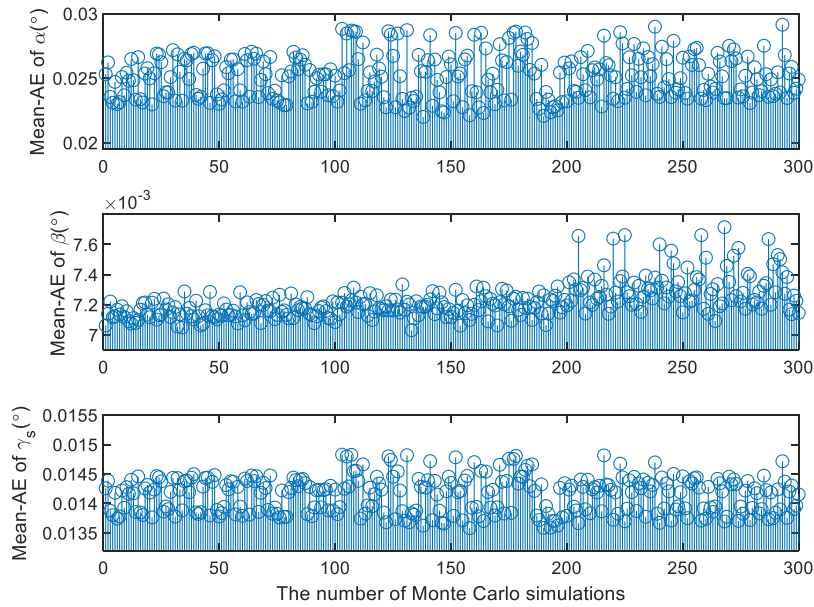


Fig. 14. Statistical charts of the Mean-AE index for the Monte Carlo results.

Table 5

Comparison of the Monte Carlo results of the number of communication events of the QFFCL with and without the HQ.

Index	Channel	QFFCL (with HQ)	QFFCL (without HQ)	Increment (%)
Number of communication events (Integer average of 300 Monte Carlo results)	δ_e	1043	1500	-30.47
	δ_a	1055	1500	-29.67
	δ_r	979	1500	-34.73
	Total	3077	4500	-31.62

the HQ, which demonstrates the effectiveness of the HQ. In summary, the Monte Carlo simulation results demonstrate the robustness and effectiveness of the proposed control scheme.

5. Conclusion

To address the attitude tracking problem of hypersonic reentry vehicles (HRVs), a quantized fixed-time fault-tolerant attitude control scheme is proposed. First, the model of the HRV is established in the presence of time-varying actuator faults, uncertainties, external disturbances, signal quantization, and limited communication capacity. Then, fixed-time extended state observers are employed to estimate the lumped disturbances within a fixed time. Moreover, the quantized fixed-time fault-tolerant control laws are designed to guarantee the control performance. The simulation results illustrate the superiority and robustness of the proposed control strategy. More specifically, by comparing with the mean absolute error and max absolute error indexes of the comparison methods [21,38], the performance of the proposed control scheme is improved by more than 25.71%. Under the effect of the hysteresis quantization mechanism, the number of communication events is reduced by about 31.62%, which effectively reduces the communication load and saves communication resources.

In addition, we intend to consider the following directions in the future:

- (1) To consider the real health statuses of the actuators, a real-time fault-diagnosis-based fault-tolerant control scheme for HRVs will be further studied.
- (2) Some issues in the actual control process, such as sensor noise and transmission delay, will be further considered.
- (3) A practical testing platform composed of a server, an industrial PC, and a high-value embedded controller will be established in the future, and related flight tests will be carried out to validate the performance of the proposed control strategy.

Acknowledgements

The authors especially like to thank the Editor-in-Chief, the Associate Editor, and the anonymous reviewers for their comments and suggestions that helped to improve the paper significantly.

This work is funded in part by the Aeronautical Science Foundation of China under Grant no. 2018ZC51031, in part by the National Natural Science Foundation of China under Grant no. 61673042. This research is also supported by the high-performance computing (HPC) resources at Beihang University.

References

- [1] Z. Guo, J. Zhou, J. Guo, J. Cieslak, J. Chang, Coupling-Characterization-Based Robust Attitude Control Scheme for Hypersonic Vehicles, *IEEE Trans. Ind. Electron.* 64 (2017) 6350–6361.
- [2] Y. Shi, X. Shao, W. Zhang, Quantized learning control for flexible air-breathing hypersonic vehicle with limited actuator bandwidth and prescribed performance, *Aerosp. Sci. Technol.* 97 (2020) 105629.
- [3] X. Shao, H. Wang, Active disturbance rejection based trajectory linearization control for hypersonic reentry vehicle with bounded uncertainties, *ISA Trans* 54 (2015) 27–38.
- [4] X. Bu, X. Wu, R. Zhang, Z. Ma, J. Huang, Tracking differentiator design for the robust backstepping control of a flexible air-breathing hypersonic vehicle, *J. Frankl. Inst.* 352 (2015) 1739–1765.
- [5] H. Sun, S. Li, C. Sun, Finite time integral sliding mode control of hypersonic vehicles, *Nonlinear Dyn* 73 (2013) 229–244.
- [6] M.V. Basin, P. Yu, Y.B. Shtessel, Hypersonic missile adaptive sliding mode control using finite- and fixed-time observers, *IEEE Trans. Ind. Electron.* 65 (2018) 930–941.
- [7] L. Fiorentini, A. Serrani, M.A. Bolender, D.B. Doman, Nonlinear robust adaptive control of flexible air-breathing hypersonic vehicles, *J. Guid. Control Dyn.* 32 (2009) 402–417.
- [8] H.-N. Wu, S. Feng, Z.-Y. Liu, L. Guo, Disturbance observer based robust mixed H_2/H_∞ fuzzy tracking control for hypersonic vehicles, *Fuzzy Sets Syst* 306 (2017) 118–136.
- [9] Y. Wang, X. Yang, H. Yan, Reliable fuzzy tracking control of near-space hypersonic vehicle using aperiodic measurement information, *IEEE Trans. Ind. Electron.* 66 (2019) 9439–9447.
- [10] B. Xu, D. Wang, Y. Zhang, Z. Shi, DOB-based neural control of flexible hypersonic flight vehicle considering wind effects, *IEEE Trans. Ind. Electron.* 64 (2017) 8676–8685.
- [11] R. Chai, A. Tsourdos, A. Savvaris, Y. Xia, S. Chai, Real-time reentry trajectory planning of hypersonic vehicles: a two-step strategy incorporating fuzzy multiobjective transcription and deep neural network, *IEEE Trans. Ind. Electron.* 67 (2020) 6904–6915.
- [12] R. Chai, A. Tsourdos, A. Savvaris, S. Chai, Y. Xia, C.L.P. Chen, Six-DOF spacecraft optimal trajectory planning and real-time attitude control: a deep neural network-based approach, *IEEE Trans. Neural Netw. Learn. Syst.* 31 (2020) 5005–5013.
- [13] R. Chai, A. Tsourdos, A. Savvaris, S. Chai, Y. Xia, C.L.P. Chen, Design and implementation of deep neural network-based control for automatic parking maneuver process, *IEEE Trans. Neural Netw. Learn. Syst.* (2020) 1–14.
- [14] X. Yu, Z. Liu, Y. Zhang, Fault-tolerant flight control design with finite-time adaptation under actuator stuck failures, *IEEE Trans. Control Syst. Technol.* 25 (2017) 1431–1440.
- [15] C. Wang, L. Guo, C. Wen, Q. Hu, J. Qiao, Event-triggered adaptive attitude tracking control for spacecraft with unknown actuator faults, *IEEE Trans. Ind. Electron.* 67 (2020) 2241–2250.
- [16] H. An, J. Liu, C. Wang, L. Wu, Approximate back-stepping fault-tolerant control of the flexible air-breathing hypersonic vehicle, *IEEE-ASME Trans. Mechatron.* 21 (2016) 1680–1691.
- [17] Q. Hu, C. Wang, Y. Li, J. Huang, Adaptive control for hypersonic vehicles with time-varying faults, *IEEE Trans. Aerosp. Electron. Syst.* 54 (2018) 1442–1455.
- [18] B. Xu, Z. Shi, F. Sun, W. He, Barrier Lyapunov function based learning control of hypersonic flight vehicle with AOA constraint and actuator faults, *IEEE T. Cybern.* 49 (2019) 1047–1057.
- [19] H. Xu, M.D. Mirmirani, P.A. Ioannou, Adaptive sliding mode control design for a hypersonic flight vehicle, *J. Guid. Control Dyn.* 27 (2004) 829–838.
- [20] X. Yu, P. Li, Y. Zhang, Fixed-time actuator fault accommodation applied to hypersonic gliding vehicles, *IEEE Trans. Autom. Sci. Eng.* (2020) 1–12.
- [21] X. Yu, P. Li, Y. Zhang, The design of fixed-time observer and finite-time fault-tolerant control for hypersonic gliding vehicle, *IEEE Trans. Ind. Electron.* 65 (2018) 4135–4144.
- [22] P. Li, X. Yu, Y. Zhang, X. Peng, Adaptive multivariable integral TSMC of a hypersonic gliding vehicle with actuator faults and model uncertainties, *IEEE-ASME Trans. Mechatron.* 22 (2017) 2723–2735.
- [23] X. Shao, B. Tian, W. Yang, Fixed-time trajectory following for quadrotors via output feedback, *ISA Trans.* (2020).
- [24] X. Shao, H. Si, W. Zhang, Fuzzy wavelet neural control with improved prescribed performance for MEMS gyroscope subject to input quantization, *Fuzzy Sets Syst.* (2020).
- [25] X. Shao, Y. Shi, W. Zhang, Input-and-measurement event-triggered control for flexible air-breathing hypersonic vehicles with asymmetric partial-state constraints, *Nonlinear Dyn.* 102 (2020) 163–183.
- [26] Y. Gao, J. Liu, Z. Wang, L. Wu, Interval Type-2 FNN-based quantized tracking control for hypersonic flight vehicles with prescribed performance, *IEEE Trans. Syst. Man Cybern. -Syst.* (2019) 1–13.
- [27] B. Tian, H. Lu, Z. Zuo, W. Yang, in: Fixed-Time Leader-Follower Output Feedback Consensus For Second-Order Multiagent Systems, 49, *IEEE T. Cybern.* 2019, pp. 1545–1550.
- [28] S. Keshmiri, R. Colgren, M. Mirmirani, Development of an aerodynamic database for a generic hypersonic air vehicle, in: *AIAA Guidance, Navigation, and Control Conference and Exhibit*, 2005, p. 6257.
- [29] S. Keshmiri, M. Mirmirani, R. Colgren, Six-DOF modeling and simulation of a generic hypersonic vehicle for conceptual design studies, in: *AIAA Modeling and Simulation Technologies Conference and Exhibit*, 2004, p. 4805.
- [30] J. Zhou, C. Wen, W. Wang, Adaptive control of uncertain nonlinear systems with quantized input signal, *Automatica* 95 (2018) 152–162.
- [31] F. Wang, B. Chen, C. Lin, J. Zhang, X. Meng, Adaptive neural network finite-time output feedback control of quantized nonlinear systems, *IEEE Trans. Cybern.* 48 (2018) 1839–1848.
- [32] Y. Yu, H. Wang, N. Li, H. Zhang, Z. Su, X. Shao, Finite-time model-assisted active disturbance rejection control with a novel parameters optimizer for hypersonic reentry vehicle subject to multiple disturbances, *Aerosp. Sci. Technol.* 79 (2018) 588–600.
- [33] X. Wang, J. Guo, S. Tang, S. Qi, Fixed-time disturbance observer based fixed-time back-stepping control for an air-breathing hypersonic vehicle, *ISA Trans* 88 (2019) 233–245.
- [34] J. Zhang, S. Yu, Y. Yan, Fixed-time output feedback trajectory tracking control of marine surface vessels subject to unknown external disturbances and uncertainties, *ISA Trans.* 93 (2019) 145–155.
- [35] M. Basin, P. Yu, Y. Shtessel, Finite- and fixed-time differentiators utilising HOSM techniques, *IET Contr. Theory Appl.* (2017) 1144–1152.
- [36] B. Jiang, Q. Hu, M.I. Friswell, Fixed-time attitude control for rigid spacecraft with actuator saturation and faults, *IEEE Trans. Control Syst. Technol.* 24 (2016) 1892–1898.
- [37] Z. Zuo, Nonsingular fixed-time consensus tracking for second-order multi-agent networks, *Automatica* 54 (2015) 305–309.
- [38] Y. Yu, H. Wang, N. Li, Fault-tolerant control for over-actuated hypersonic reentry vehicle subject to multiple disturbances and actuator faults, *Aerosp. Sci. Technol.* 87 (2019) 230–243.